Stanford Geothermal Program
Interdisciplinary Research
in Engineering and Earth Sciences
Stanford University
Stanford, California

# HEAT AND MASS TRANSFER IN POROUS ROCK FRAGMENTS

by
M. C. T. Kuo
P. Kruger
W. E. Brigham

December, 1975

This research was carried out
under Research Grant AER-72-03490
by the National Science Foundation

# ABSTRACT

Fracture stimulation is expected to increase the productivity of geothermal reservoirs by providing increased permeability in hydrothermal systems or increased surface area for heat transfer in hot igneous systems. The extent of heat and mass transfer from porous rock fragments to circulating fluids is important for evaluating the effects of fracture stimulation. Experimental data have been obtained for individual spherical porous rocks. The rate of mass transfer between tritiated-water saturated rock to surrounding fluid was determined by radioactivity measurement. The rate of heat transfer was determined by quartz thermometry.

The measured effective mass diffusivity of the micropore water was of the order of $10^{-6}$ cm$^2$/sec and the measured thermal diffusivity of the rock fragments was of the order of $10^{-2}$ cm$^2$/sec. These data were used to analyze energy transfer for a model involving both intrasphere and interface transport steps. The results show that heat transfer is the dominant mechanism for transferring energy from hot porous spheres to circulating cold water at constant pressure.

# ACKNOWLEDGMENTS

The authors express their appreciation to Professor A. L. London for his stimulation and assistance during the course of this work. The research was supported by the National Science Foundation under Grant No. AER-72-03490.

# TABLE OF CONTENTS

## NOMENCLATURE

English Letter Symbol:;

$A$ = area ($ft^2$).

$C$ = concentration of tritiated water (cpm/mℓ).

$C$ = heat capacity (Btu/°F).

$C_p$ = specific heat capacity (Btu/lb °F).

$D$ = molecular diffusivity ($cm^2$/sec).

$D$ = diameter of porous sphere (in).

$D_e$ = effective molecular diffusivity in porous media (cm2/sec).

Fr = Fourier number (dimensionless).

$h$ = heat transfer coefficient (Btu/hr °F-ft2).

$k$ = thermal conductivity (Btu/°F-ft).

$M$ = mass (lb).

Nu = Nusselt number (dimensionless).

Pr = Prandtl number

$q$ = energy transfer rate (Btu/hr).

$R$ = radius of sphere (in).

Re = Reynolds number (dimensionless).

$r$ = radius from the center of sphere.

Sc = Schmidt number (dimensionless).

Sh = Sherwood number (dimensionless)

$T$ = temperature (°F or °C).

$V$ = volume ($ft^3$).

$W$ = weight (g).

## Greek Letter Symbols

$\alpha$ = thermal diffusivity ($cm^2/sec$).

$\theta$ = time (sec or min).

$\rho$ = density ($lb/ft^3$).

$\phi$ = porosity (dimensionless).

$\omega$ = capacity ratio (dimensionless).

## Subscripts

c = core.

f = fluid.

i = initial.

m = mass transfer mechanism.

s = sphere.

t = heat transfer mechanism.

= infinite time.

## Superscript

$*$ = dimensionless quantity.

# CHAPTER 1

# INTRODUCTION

Vast quantities of thermal energy are stored in the earth's crust. The development of geothermal energy resources may contribute between 0.2 and 8 percent of the U.S. electric generating capacity by 1985, and between 1.5 and 14.4 percent in the year 2000 (U.S. Department of the Interior, 1973). Currently, only the highest quality hydrothermal resources are utilized commercially for the generation of electric power. For significant contribution from lower temperature hydrothermal systems and such systems as geopressured basins and hot dry rock, development of new technologies is needed if these promising estimates are to be translated into reality. For long-term economic viability, stimulation technology of hydrothermal and hot dry rock reservoirs will be required.

Stimulation of geothermal reservoirs can be useful to improve the performance of natural reservoirs or to create usable reservoirs in otherwise unexploitable geothermal resources (Ewing, 1973). The use of chemical explosives for stimulation of marginal geothermal wells has been suggested by Austin and Leonard (1973). Hydraulic fracturing, thermal stress cracking (Smith et al., 1973), and nuclear explosive fracturing (Burnham and Stewart, 1973) have been proposed for hot dry rock formations. The major effects of fracturing or cracking include increased formation permeability and increased surface area of hot dry rock. Ramey and Kruger and Raghavan (1973) proposed high-yield explosives to create a rubble chimney in hydrothermal reservoirs. They showed from the available energy aspects of hydrothermal reservoirs, given in Table 1.1, that most

TABLE 1.1

Available Energy Content for Hypothetical Geothermal Reservoirs

| | Steam Reservoir | | | Hot-Water Reservoir | | |
|---|---|---|---|---|---|---|
| | Mass | Available Energy | | Mass | Available Energy | |
| Component | ($10^6$ lb) | ($10^6$ Btu) | (bbl oil) | ($10^6$ lb) | ($10^6$ Btu) | (bbl oil) |
| Aquifer rock | 5.410 | 233 | 40 | 5.410 | 233 | 40 |
| Fluid | 0.016 | 15 | 3 | 0.534 | 101 | 18 |
| TOTAL | 5.426 | 248 | 43 | 5.944 | 334 | 58 |

Note: Data based on a geothermal reservoir of 25 percent porosity 1 acre-foot in extent, initially at 500°F, with production at delivery pressure of 100 psia (327.8°). Oil density 340 lb/bbl.

of the available energy resides in the rock matrix rather than in the geofluid.

Production methods permitting the recovery of the heat in the rock, as well as the heat in the fluid, are under investigation (Kruger and Ramey, 1974). Fractured and porous rocks in a stimulated geothermal reservoir (chimney) contain two types of void space: (1) macropores, defined as void volume between rock fragments, and (2) micropores, defined as pore space inside individual rock fragment. Micropores may be due either to natural porosity or to induced fractures. Heat may be recovered from the rock itself by one of two processes: (1) flashing the existing liquid to steam within the pore space, or (2) recycling colder fluid back into the formation. Recycling flow of colder fluid through rock fragments is expected primarily through the macropores. Heat transfer from porous or fractured rocks to recharge fluid is a two-step process. First, heat inside the rock is conducted to the rock surface, which is then convected by surrounding fluid. In addition to heat transfer, energy extraction rate may also be significantly increased by mass transfer of hot water in the micropores to the circulating water in the macropores. The mass transfer rate is dependent on micropore porosity and permeability of the rock fragments; and the heat transfer rate is dependent on the flow regime in the macropores. Both conduction and convection have been extensively examined in the literature. However, the relative importance of mass transfer for increasing the energy extraction rate in a fractured geothermal reservoir is not well known. Therefore, the objective of this study is to assess the relative importance of mass transfer between hydrothermal fluids inside micropores of individual rocks or fragments and colder water flowing through macropores on the rate of energy transfer to the macropore water in a stimulated geothermal reservoir.

The study of heat and mass transfer inside a fractured geothermal reservoir can be simplified by measurement of heat and mass transfer rate from single rocks to surrounding fluid. The results from single rock studies can be extended to a reservoir system. To evaluate the important mechanisms related to heat extraction from highly fractured or porous medius, separate experiments were conducted to determine the mass transfer and the heat transfer rates from well-defined artificial porous rocks to surrounding fluid under controlled transient conditions. The experiments encompassed the following specific objectives:

(1) experimental determination of the mass transfer rate between micropore water of individual porous rocks and the surrounding macropore water. Tritiated water was used as the experimental label for the micropore water.

(2) experimental determination of the heat transfer rate from individual water-saturated hot porous rocks to colder surrounding water. A quartz thermometer was used to monitor the temperature of surrounding water.

(3) assessment of the importance of mass transfer on the rate of energy transfer based on these experimental data.

Rocks of spherical shape are more readily amenable to mathematical analysis. Therefore, fabricated porous rocks of spherical shape were used in the experiments. Mathematical models were designed to represent the physical systems. The models express mass and heat transfer rates in terms of mass and thermal diffusivity. The mass and thermal diffusivity were estimated from the comparison of experimental data with mathematical models. The relative importance of mass and heat transfer were assessed based on the estimated values of mass and thermal diffusivity.

# CHAPTER 2

# EXPERIMENTAL TECHNIQUES

In these mass and heat transfer experiments, an artificial porous sphere was immersed in a cylinder of surrounding fluid and the mass or heat transfer rates were determined by periodic sampling and measurement of the corresponding tracer concentration or fluid temperature. Since the measurements involved small changes in tracer concentration and temperature, methods of high sensitivity and precision were required.

For mass transfer experiments involving water, tritium in the form of HTO is an ideal tracer because it is chemically and physically similar to water. The liquid scintillation counter is ideally suited to measure tritiated water in low concentrations. For heat transfer experiments, the quartz thermometer is also ideally suited because of its high resolving power and short time constant.

## 2.1 Preparation of Porous Sp'heres

Synthetic rocks with predictable porosity and permeability can be prepared from mixtures of sand, cement and water (Wygal, 1963; Heath, 1965; Arihara, 1974). Synthetic spherical rocks prepared **far** this study in a way similar to that of Arihara (1974) are shown in Fig. 2.1.

Fondu calcium aluminate cement, silica sand, and water were used to make the synthetic spheres in proportions of 80% sand and 20% cement by weight. The sand-cement mixture was thoroughly mixed with blending water (1% by weight) and poured into a mold of two semispheres. During the pouring the mold was tapped and vibrated from time to time in order to

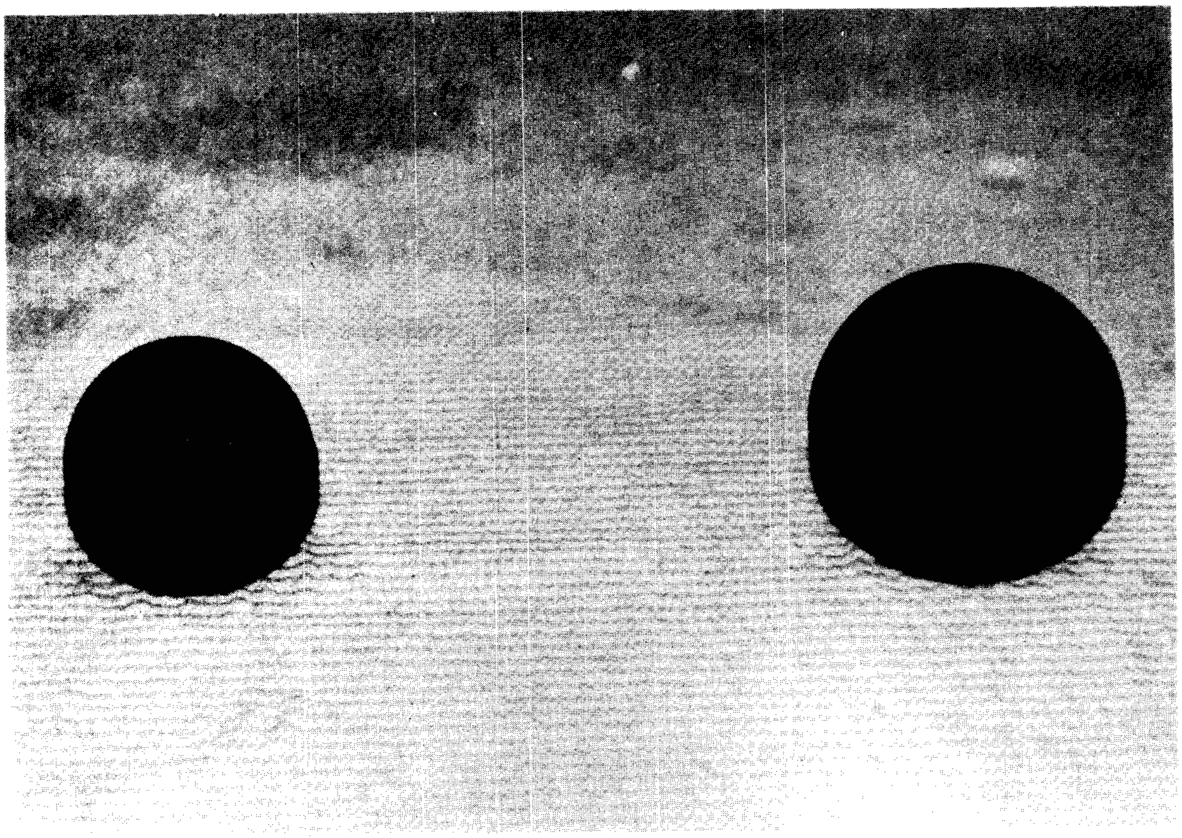

Figure 2.1 View of porous spheres

compact the sand. Water was injected through a fitting connected to one end of the mold. After breakthrough of the injected water, the mold was disconnected from the water inlet and allowed to hydrate for one day. Then the mold **was** peeled off, and the sphere was machined (filled) to shape.

Figure 2.2 shows the soaking curve of a dry porous rock in water. It can be seen that after four hours of soaking the weight of the water-saturated phere is essentially constant. The porosity of the synthetic porous rock is calculated from the difference of the measured weights of dry and saturated rock divided by the bulk volume of the sphere.

The porosity and other physical properties for the synthetic porous sphere used in this study are listed in Table 2.1. The permeability of these spheres is estimated to range from 0.09 to 0.10 darcy based on data from Arihara (1974).

TABLE 2.1

Physical Data for the Spheres

| Sphere No. | Diameter in. | Porosity % | Weight of Sand $SiO_2$, g | Weight of Cement $CaO \cdot Al_2O_3$, g | Heat Capacity* $C_s$, Btu/°F |
|---|---|---|---|---|---|
| S-1 | 2.0 | 21.4 | 101.8 | 25.5 | 0.0857 |
| S-2 | 2.0 | 16.6 | 116.0 | 29.0 | 0.0858 |
| L-1 | 2.5 | 27.7 | 185.4 | 46.3 | 0.1790 |

* Heat capacity, $C_s$, is calculated by: $C_s$ = (weight of sand)x(specific heat of sand) + (weight of cement)x(specific heat of cement) + (weight of pore water)x(specific heat of water).
The following values are used in the calculation: specific heat of sand = 0.187 cal/g°C , specific heat of cement = 0.2 cal/g°C , specific heat of water = 1.0 cal/g°C .

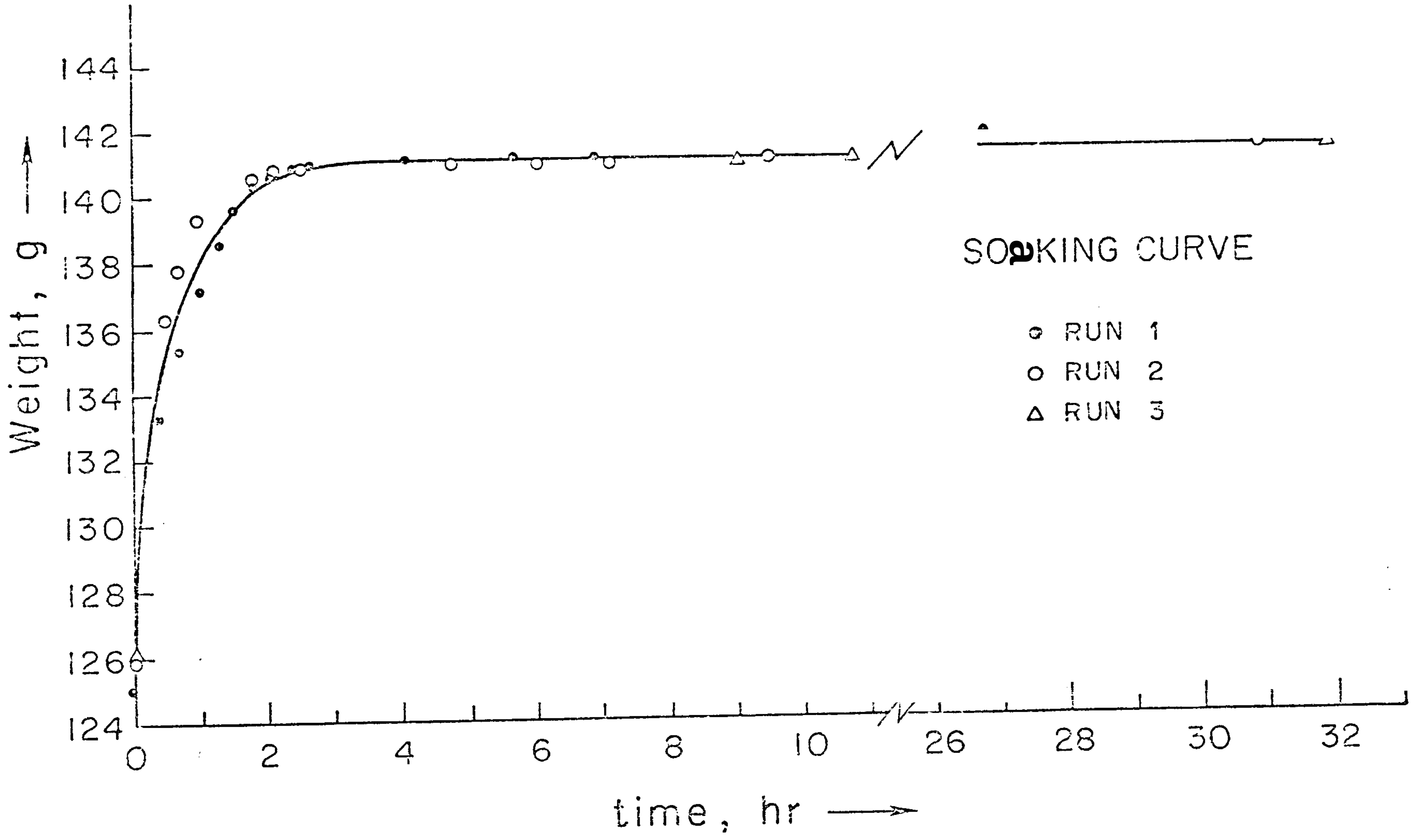

Figure 2.2 Soaking curves of a dry porous sphere

## 2.2 Mass Transfer Experiment

Three spheres of different porosity were used to determine the effect of porosity on the mass transfer rate.

### 2.2.1 Experimental System

Figure 2.3 shows the experimental system for the mass transfer experiment. The main part of the system is a large clylinder in which diffusion of the saturated tritiated water from the porous sphere into the surrounding water can be measured. The surrounding water is mixed by a magnetic stirrer to obtain uniform concentration continuously. The cylinder is temperature controlled by circulating constant-temperature water through the cylinder jacket.

### 2.2.2 Experiment Procedure

Measurement of the rate of diffusion was obtained with the following steps:

1. The synthetic prorous sphere was dried in a vacuum oven at 100°C for 20 to 30 hours until a constant weight was attained.
2. The dry sphere was immersed in a tritiated-water reservoir for at least nine hours to obtain a constant weight saturated sphere.
3. The HTO-saturated sphere was placed rapidly into the cylinder filled with pure water, at which time recording of the mass transfer rate was initiated.
4. Sample of 1 mℓ were taken from the diffusion cylinder periodically at recorded times over a fourteen-day period.
5. The samples were prepared for tritium concentration measurement in a scintillation fluid composed of the 1-mℓ sample and 10-mℓ INSTA-GEL in a 20-mℓ polyethylene vial.

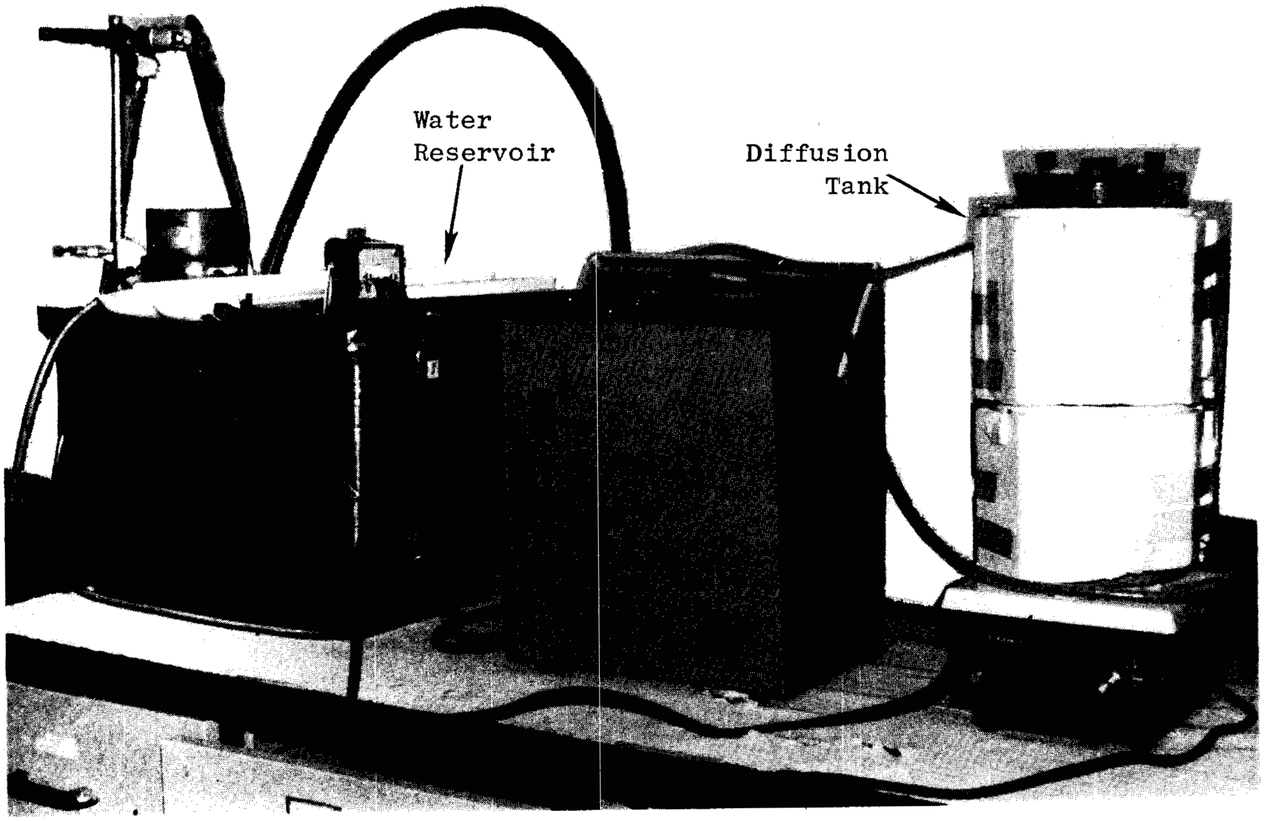

Figure 2.3 Experimental setup for mass transfer experiments

6. The tritium concentration of the sample was measured in a liquid scintillation counter (Packard Model 3330).

### 2.2.3 Tritiated Water Measurement

In a tritiated water molecule, one atom of tritium ($^{3}H$, $T_{1/2}$ = 12.3 yr, $E_{\beta^-}(max)$ = 0.0186 MeV; No $\gamma$) replaces one atom of hydrogen, $^{1}H$ . The long half life of $^{3}H$ makes its measurement by half-life determination impractical, the very weak beta-ray energy makes its measurement in regular ionization counters difficult, and since $^{3}H$ does not emit $\gamma$-radiation, y-spectroscopy cannot be used. The best form of measurement of "weak beta emitting" radioisotopes, such as $^{3}H$, is the liquid scintillation counter in which the $\beta$-particle energy is converted directly into light energy in a scintillation solution (Horrocks, 1973; Kelly and Phillips , 1973).

A scintillation sample consists of three components, the radioactive material, an organic solvent, and phosphors. The liquid scintillation process may be considered as a series of energy transfer steps mediated by an aromatic solvent and fluorescent substances called phosphors. The process may be represented by the following sequence of reactions:

(1) $\beta^- + \text{solvent} \rightarrow \text{solvent}^*$ ,

(2) $\text{solvent}^* + \text{primary scintillator} \rightarrow \text{primary scintillator}^* + \text{solvent}$ ,

(3) $\text{primary scintillator}^* + \text{secondary scintillator}$
$\rightarrow \text{secondary scintillator}^* + \text{primary scintillator}$ ,

(4) $\text{secondary scintillator}^* \rightarrow h\nu \text{ (light)} + \text{secondary scintillator}$ ,

where the star (*) represents the excited state.

By this process, the $-particle energy is transformed into pulses of light. The number of scintillations detected per unit time is proportional to the rate of radioactive decay by

$$C = \epsilon D ,$$

where

$C$ = counting rate, cpm ,

$D$ = disintegration rate of radioisotope, dpm , and

$\epsilon$ = efficiency of counting, c/d .

A schematic diagram of the detection system is shown in Fig. 2.4. The system consists of photomultiplier tubes, amplifier, coincidence circuit, discriminators and scaler to record the pulses. The coincidence circuit accepts only those pulses that occur simultaneously from both photomultiplier tubes and can reduce the background due to random thermal emission of electrons in the photomultiplier tubes. The thermal electrons produced in each individual tube are not simultaneous, except rarely by chance, and are rejected. Thermal noise is also decreased by cooling the photomultiplier tube to about 4°C. Pulse height analyzers with discriminators allow lower and upper limits to pulse amplitude accepted and passed on to the scaler, eliminating most of the undesirable pulses.

The tritiated water must be dissolved in the scintillation solution, since phase separation may lead to erratic counting rate and lower efficiency. For this purpose, INSTA-GEL (Packard Inst. Co.) was used to solubilize the aqueous samples (Carter and Dyke, 1973).

The efficiency of counting a solution with 10 mℓ INSTA-GEL and 1 mℓ sample was 32% for a gain setting of 50% and window setting, 50 ~ 1000 .

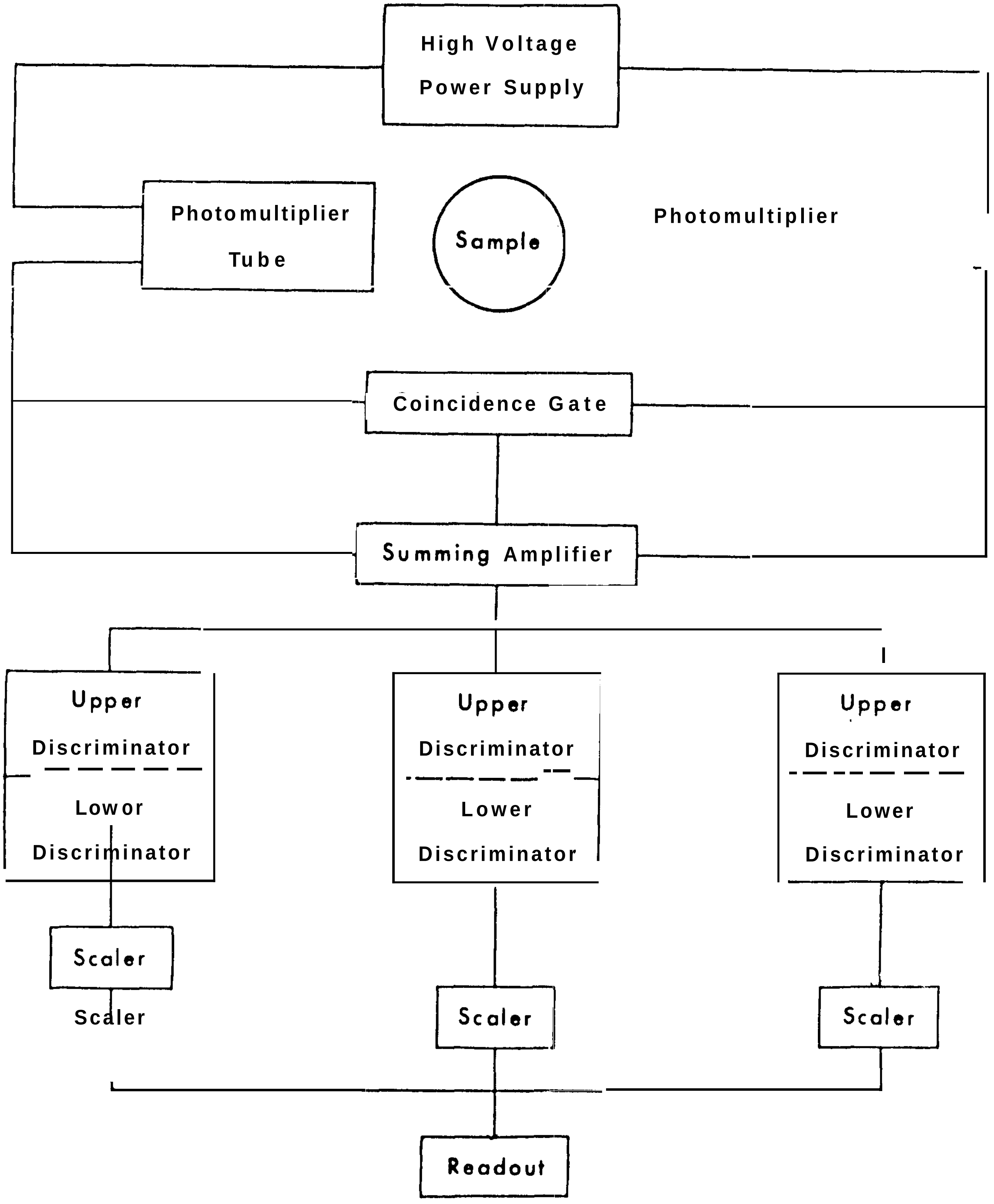

Figure 2.4 Schematic diagram of detection system of liquid scintillation counter

The background under these conditions was 11 cpm polyethylene counting vials and the minimum concentration of HTO measured was therefore about 20 to 30 cpm. The measurement uncertainties of the counting rate of the tritiated water sample are due to *two* sources: (1) natural statistical process of radioactive decay and (2) errors in pipeting volume.

The first uncertainty, due to the natural statistical process of radioactive decay, is given by the following equation (Kruger, 1971):

$$\frac{\sigma_N}{N} = \frac{1}{\sqrt{N}} = \frac{1}{\sqrt{Ct}} , \qquad (2.1)$$

where

$\sigma_N$ = standard deviation of total counts,

C = counting rate of the sample,

N = total counts,

t = counting time.

This uncertainty of counting can be reduced by increasing counting time. The second uncertainty, due to pipeting error can be estimated from sampling in triplicate by the following equations:

$$\bar{C} = \frac{C_1 + C_2 + C_3}{3} , \qquad (2.2)$$

$$\sigma_C = \sqrt{\frac{(\bar{C}-C_1)^2 + (\bar{C}-C_2)^2 + (\bar{C}-C_3)^2}{2}} , \qquad (2.3)$$

where

$C_1, C_2, C_3$ = counting rate of each sample for triple sampling,

$\bar{C}$ = mean counting rate,

$\sigma_C$ = standard deviation of counting rate.

From a mass balance of the HTO tracer, assuming no tracer is absorbed in the porous sphere, the final concentration can be predicted as

$$(C_{f\infty})_{\text{predicted}} - \frac{413\ \phi\ \pi R^3 C_{si}}{V_f + 4/3\ \phi\ \pi R^3}, \tag{2.4}$$

where

$C_{f\infty}$ = final concentration of tritiated water in the surrounding fluid,

$C_{si}$ = initial concentration of tritiated water in the sphere,

$V_f$ = volume of the surrounding fluid.,

$R$ = radius of the sphere, and

$\phi$ = porosity of the sphere.

Thus, when the concentration measured in each experiment reaches the predicted final concentration, it is concluded that the equilibrium state has been reached and affirms that no tracer has been absorbed in the porous sphere.

## 2.3 Heat Transfer Experiment

### 2.3.1 Experimental System

Figure 2.5 shows the experimental setup for the heat transfer experiment. The system includes a thermostat-controlled hot reservoir, an adiabatic cold reservoir, magnetic stirrers, and a quartz thermometer. The cold reservoir is the part of the system in which the hot sphere is introduced and the temperature response is measured. It is insulated by styrene. Adiabatic conditions were checked by cool-down testing. Three different stirrer speeds were used in the cold reservoir of surrounding water to check the effect of external flow regime on the temperature response of the surrounding water.

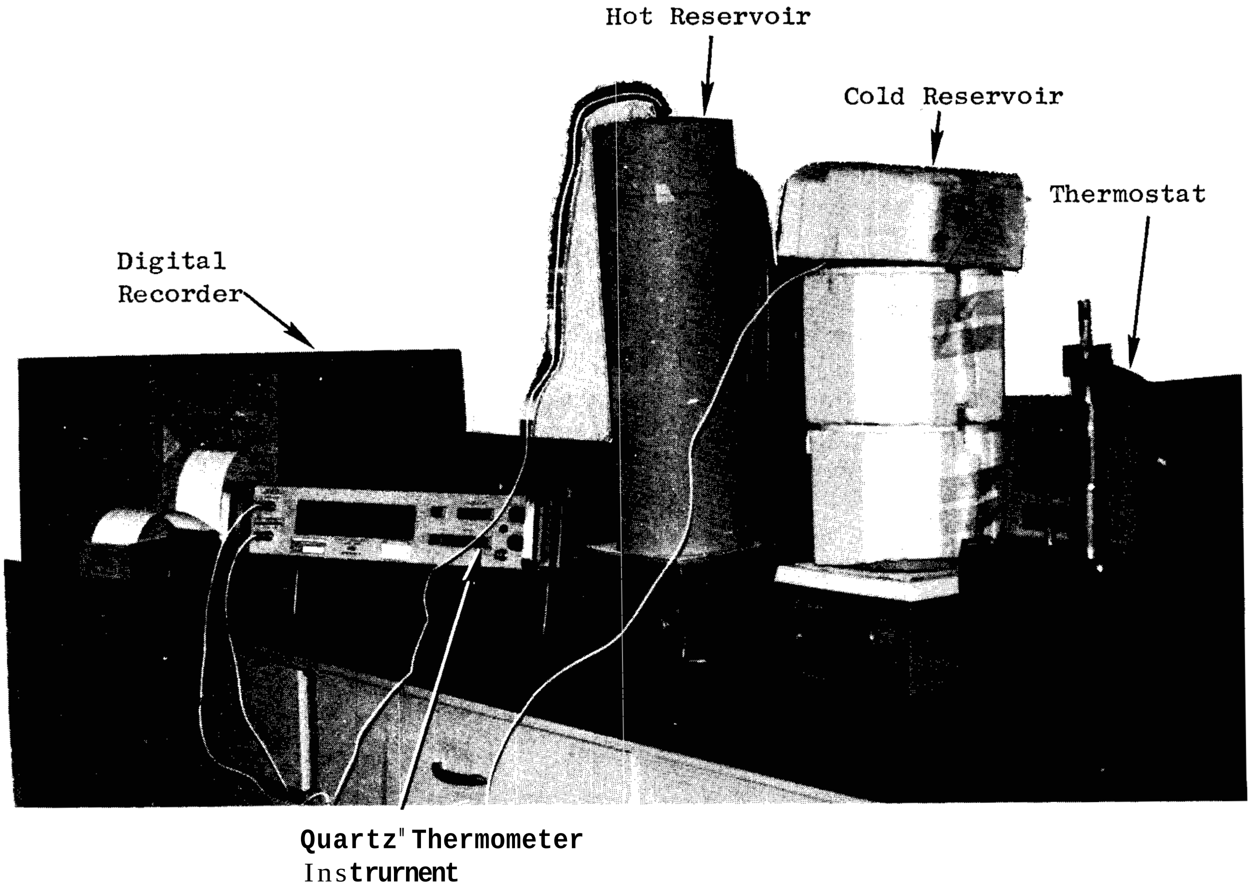

Figure 2.5 Experimental setup for heat transfer experiments

### 2.3.2 Experimental Procedure

The experimental procedure consists of the following steps:

1. The synthetic porous sphere was brought to the desired temperature (around 55°C) in the thermosrat-controlled hot reservoir.
2. The initial temperature of the sphere, $T_{si}$ , is recorded when the hot reservoir reaches the set point of the thermostat.
3. The initial temperature of the cold reservoir, $T_{fi}$ , is recorded.
4. The hot sphere is rapidly transferred to the cold reservoir which initiates the recording of external fluid temperature.
5. Temperature recording as a function of time stops when the external fluid has acquired temperature equilibrium with the porous sphere.

### 2.3.3 Temperature Measurement

The temperature rise in the surrounding water is very small compared to the temperature drop in the synthetic sphere, because the large heat capacity ratio of the surrounding water to that of the synthetic sphere. For a heat capacity ratio of 60, and a temperature difference of the sphere, $T_{si} - T_{s\infty}$ , of 30°C, the temperature difference of the surrounding water is $T_{f\infty} - T_{fi} = 0.5\,°C$ . The time constant of the heat transient behavior of a sphere of 1-inch radius is estimated to be 100 sec. Therefore, the temperature measuring system was selected on the basis of three primary criteria: high resolution, quick response, and direct recording. In this study, the resolution of 0.01°C is adopted and the uncertainty of each temperature measurement is estimated to be ± 0.01°C.

Quartz Thermometer. A quartz thermometer (Hewlett Paclcard Model 2801 A) was used in this study. It:; key features include resolution to 0.001"C, a 2-second time constant, and digital recording output. The sensor is a pure quartz crystal resonator with a natural frequency of oscillation, linearly dependent on temperature. It: oscillates at a nominal freuuency of 28 MHz at 0°C with a frequency gradient of approximately 1000 Hz per degree Celsius. The resonator is sealed in a stainless steel probe, primarily intended for liquid immersion., as shown in Fig. *2.6.* The schematic diagram of the quartz. thermometer system is shown in Fig. *2.7.* The instrument contains a sensor oscillator and a stabilized reference oscillator with which the sensor signal is compared. The reference frequency is about 28 MHz and is adjustable so that a precise zero beat can be achieved at zero degree and a slope of 1000 Hz/°C is obtained. The instrument also contains an electronic counter circuit, which detects the beats and provides the digital display.

### *2.3.4* Cool-Down Testing

The adiabatic condition of the styrene insulated cold reservoir was checked with cool-down experiments. The styrene insulated system was first heated to a high temperature condition (about 55°C) by circulating hot water through the cylinder jacket, following which the system was allowed to cool down. Temperature measurements in the system and the surrounding environment were recorded as a function of time.

A mathematical model for the cool-down transient can be obtained. from the energy balance for the experimental system. For one-lump model, the various masses of experimental system, water and glass, are assumed to be at uniform temperature. The energy balance equation for the experimental system is

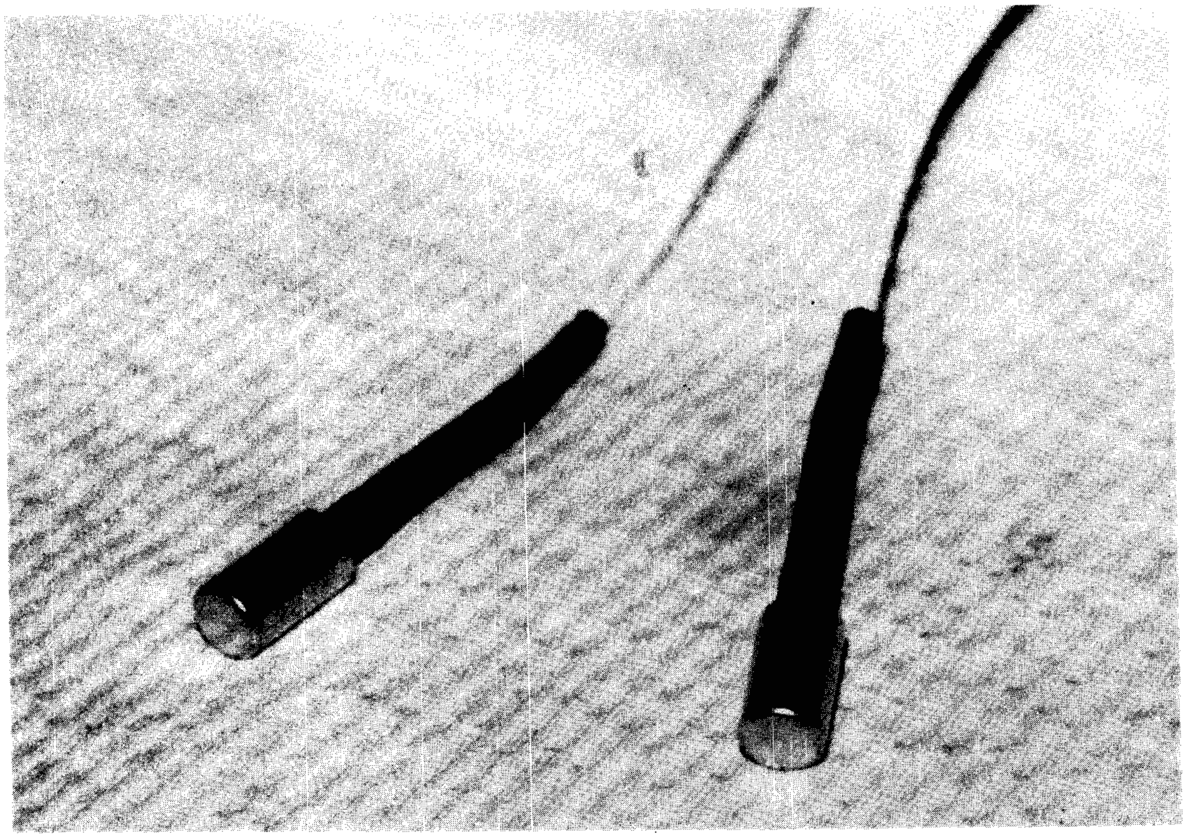

Figure 2.6 View of quartz thermometer probe

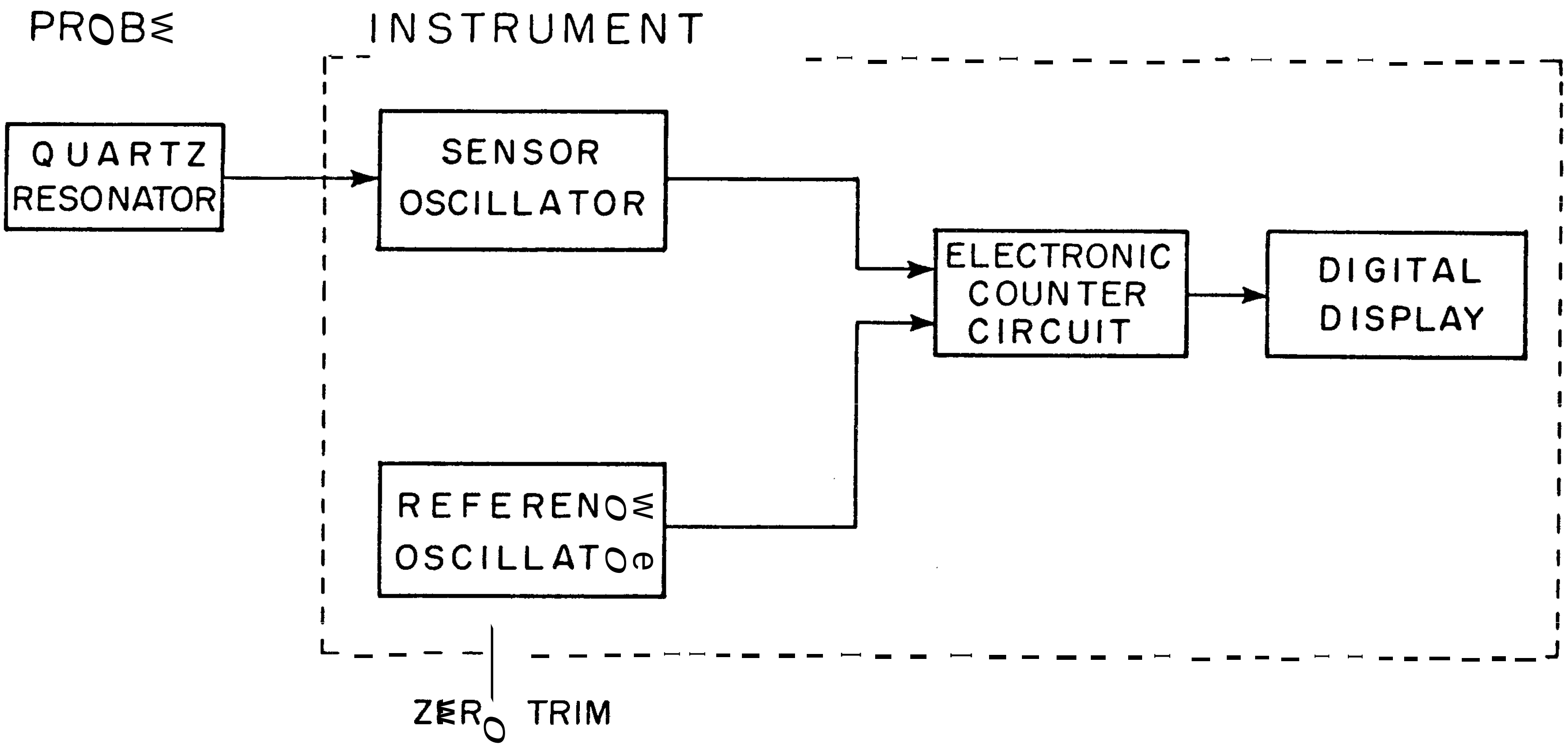

Figure 2 7 Schematic diagram of quartz thermometer system

$$MC_p \frac{dT}{d\theta} = - hA(T - T_\infty) \quad , \qquad (2.5)$$

where

$MC_p$ = heat capacity of the experimental system,
$T$ = temperature of the system,
$T_\infty$ = temperature of the environment, and
$hA$ = heat transfer parameter of the system.

Solving the above equation with the initial condition $T = T_i$ at $\theta = 0$ yields

$$\ell n(T - T_\infty) = - \frac{hA}{MC_p}\theta + \ell n(T_i - T_\infty) \quad . \qquad (2.6)$$

According to the above solution for one-lump model, the cool-down experimental data will. follow a semi-log straight line with $(T - T_\infty)$ vs. $\theta$ . The heat transfer parameter of the system, $hA$ , can be estimated from the slope of the straight line.

# CHAPTER 3

# EXPERIMENTAL RESULTS

## 3.1 Mass Transfer Data

Figures 3.1, 3.2, and 3.3 show mass transfer experimental data for three runs with three different-porosity spheres. The final concentration measured in each run reaches the predicted value based on Eq. (2.4). Therefore, no tracer (HTO) has been absorbed by the porous sphere and the equilibrium state of diffusion has been attained.

The uncertainties of the counting rate of tritiated water samples are due to two sources: (1) natural statistics of radioactive decay, and (2) errors in pipeting volume. According to Eq. (2.1) the first uncertainty of each sample was reduced to 1% by increasing counting time so that total count of each measurement equa'ls 10,000. The second uncertainty was estimated for the second and third runs (Runs MT-071775 and MT 073175) based on Eqs. (2.3) and (2.4). The first run (Run MT-121074) was single sampling and the standard deviations due to pipeting cannot be estimated. The estimated standard deviations for the second and third runs are shown in Figs. 3.2 and 3.3. Most errors due to pipeting are within 5% and can be seen from tabulated data in Appendix D.

## 3.2 Heat Transfer Data

Figures 3.4, 3.5, and 3.6 present heat transfer experiment data for four runs with three different stirrer speeds:. Tabulated data are given in Appendix E. As can be seen from these figures, there is a measured increasing rate of surrounding fluid temperature before the hot sphere

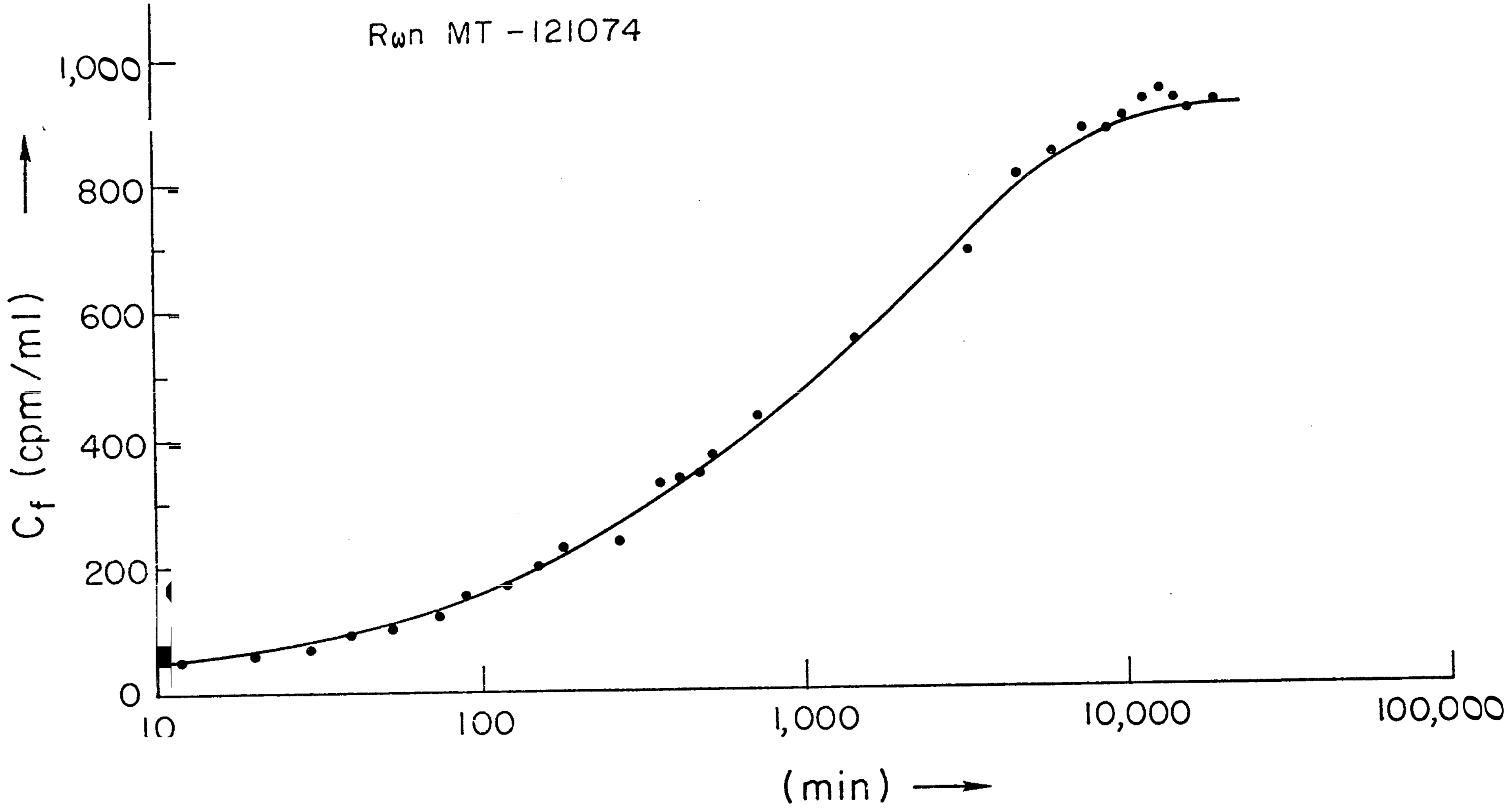

Figure 3 1 Mass transfer experiment data for Run MT-121074

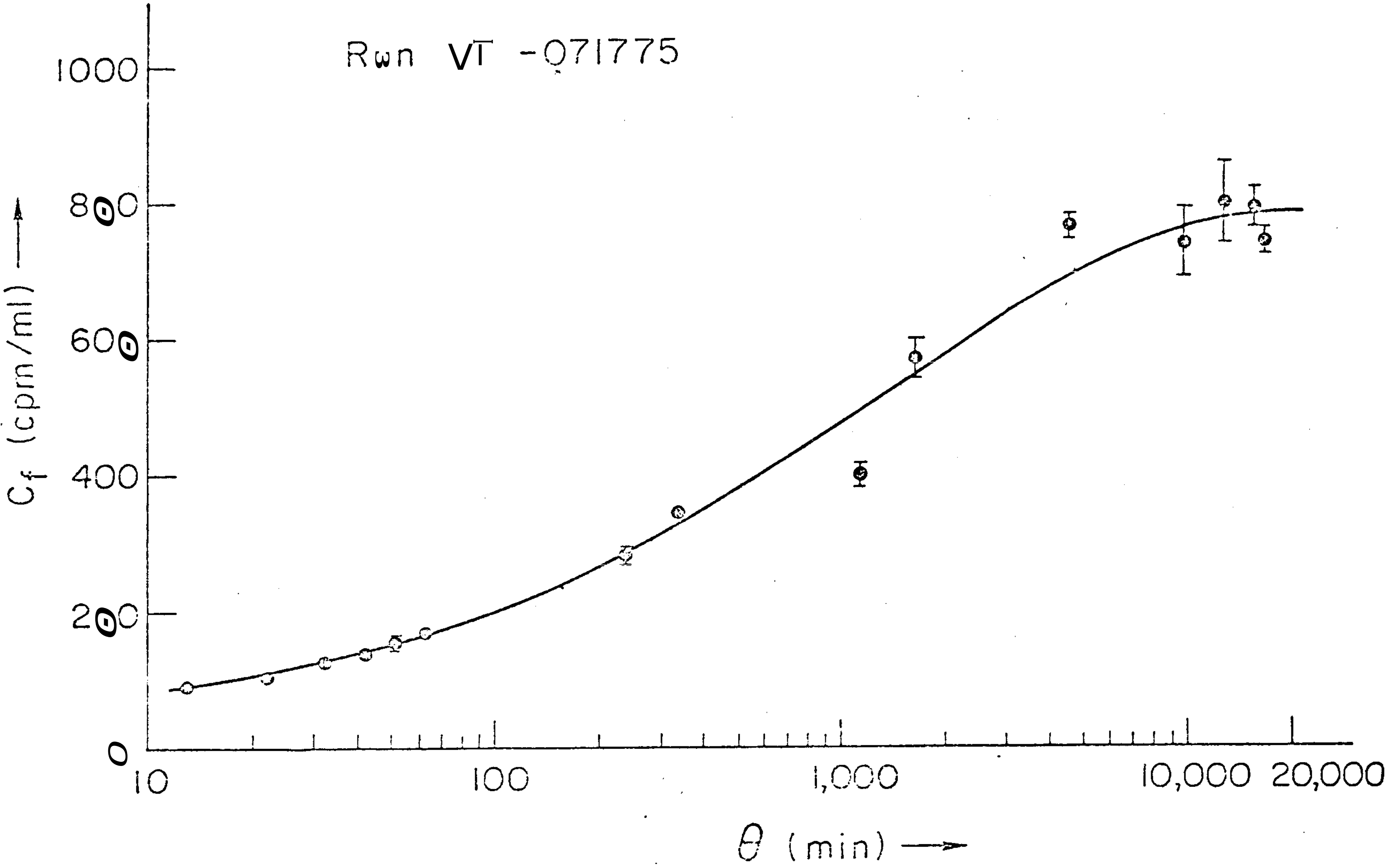

Figure 3.2 Mass transfer experiment data for Run MT-071775

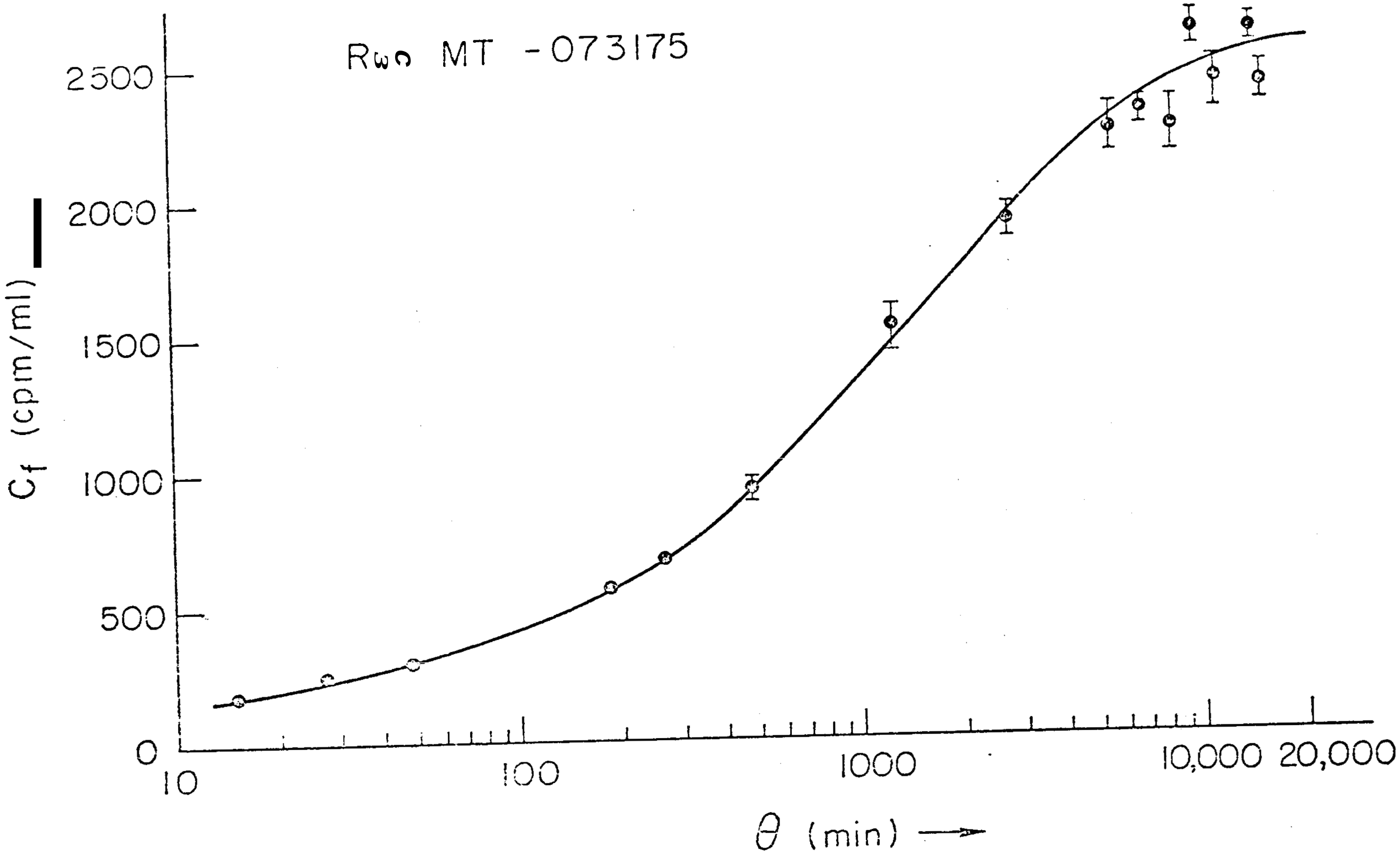

Figure 3.3   Mass transfer experiment data for Run MT-073175

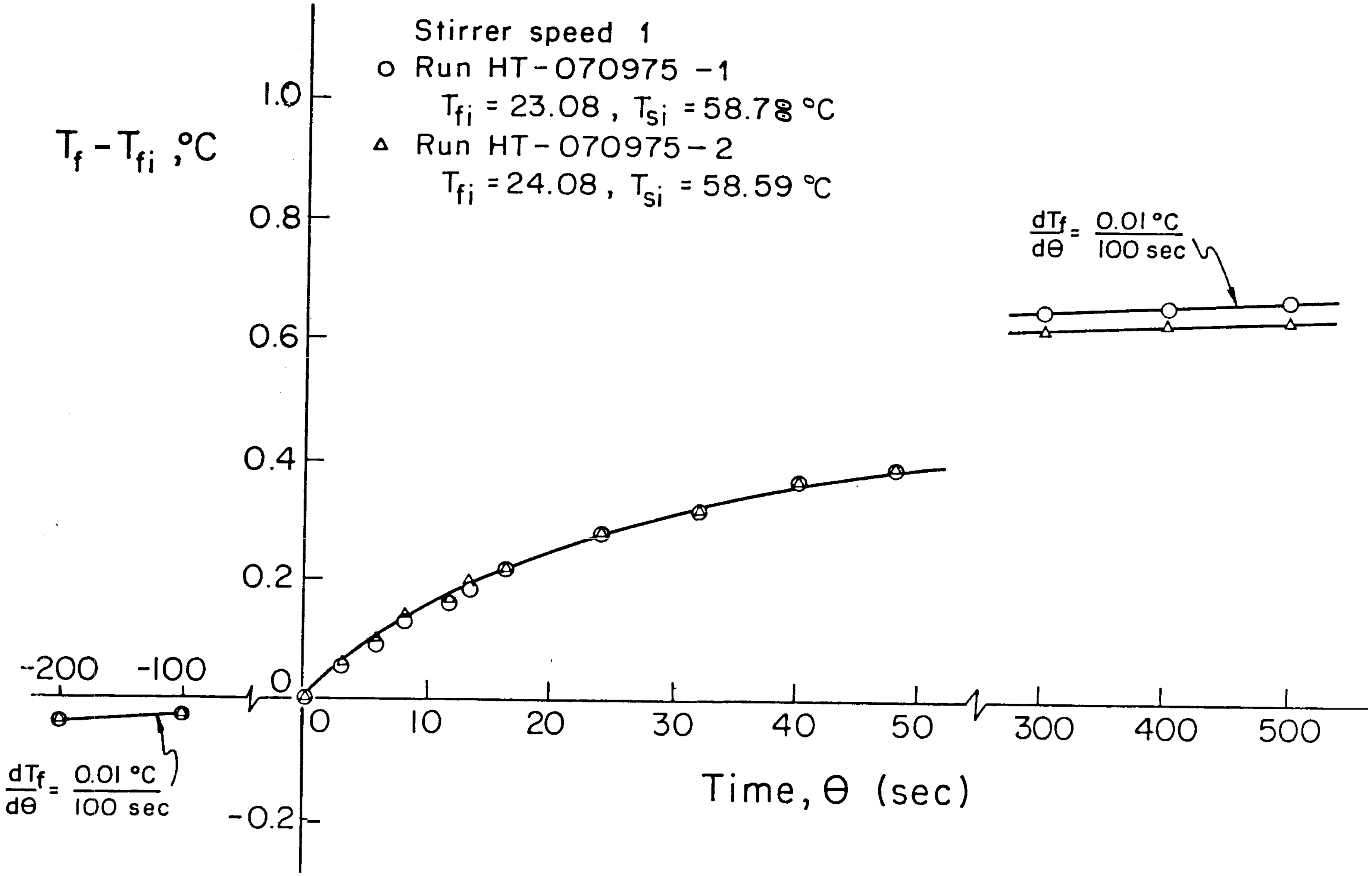

Figure 3.4 Heat transfer experiment data for Run HT-070975-1 and HT-070975-2

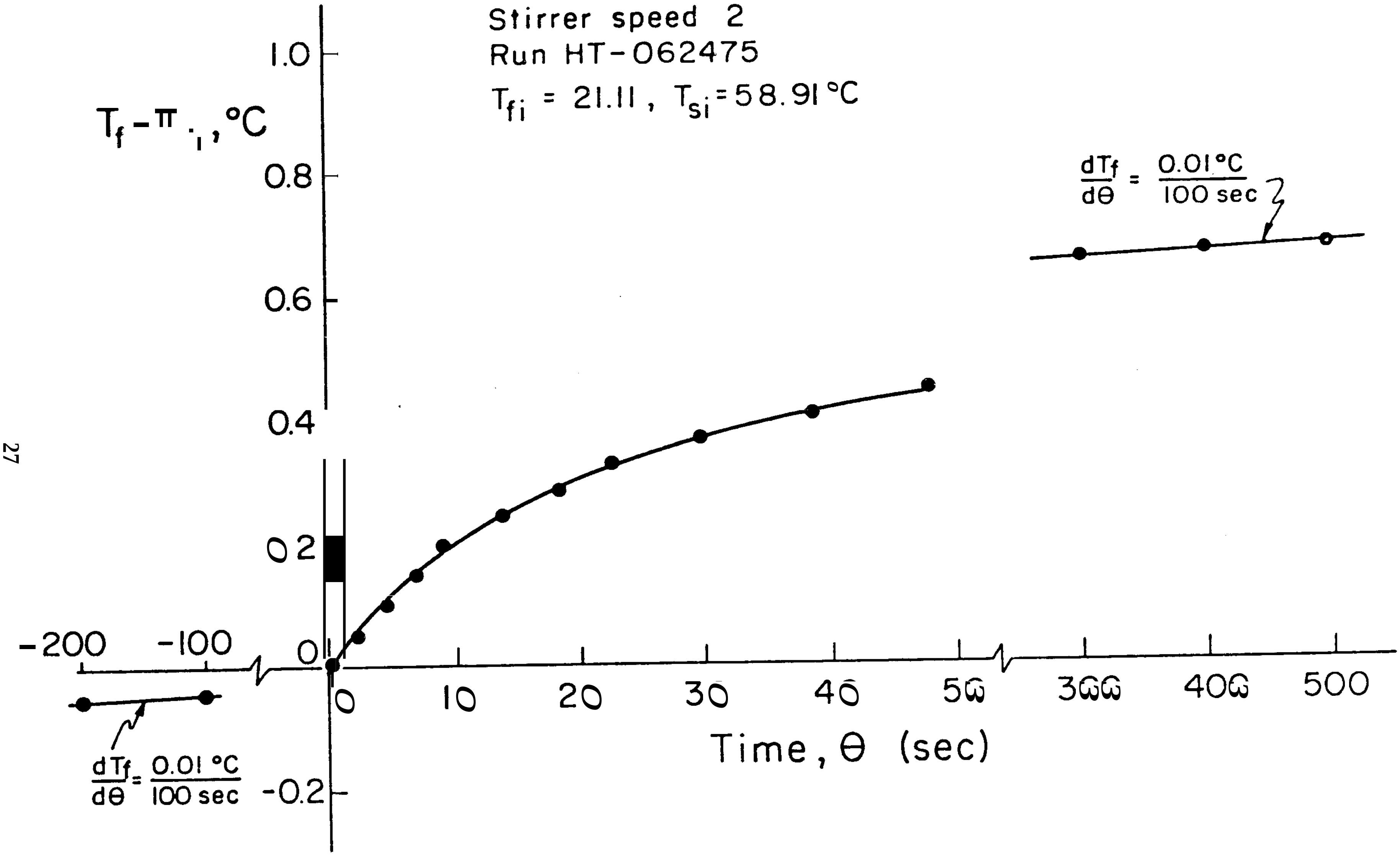

Figure 3.5 Heat transfer experiment data for Run HT-062475

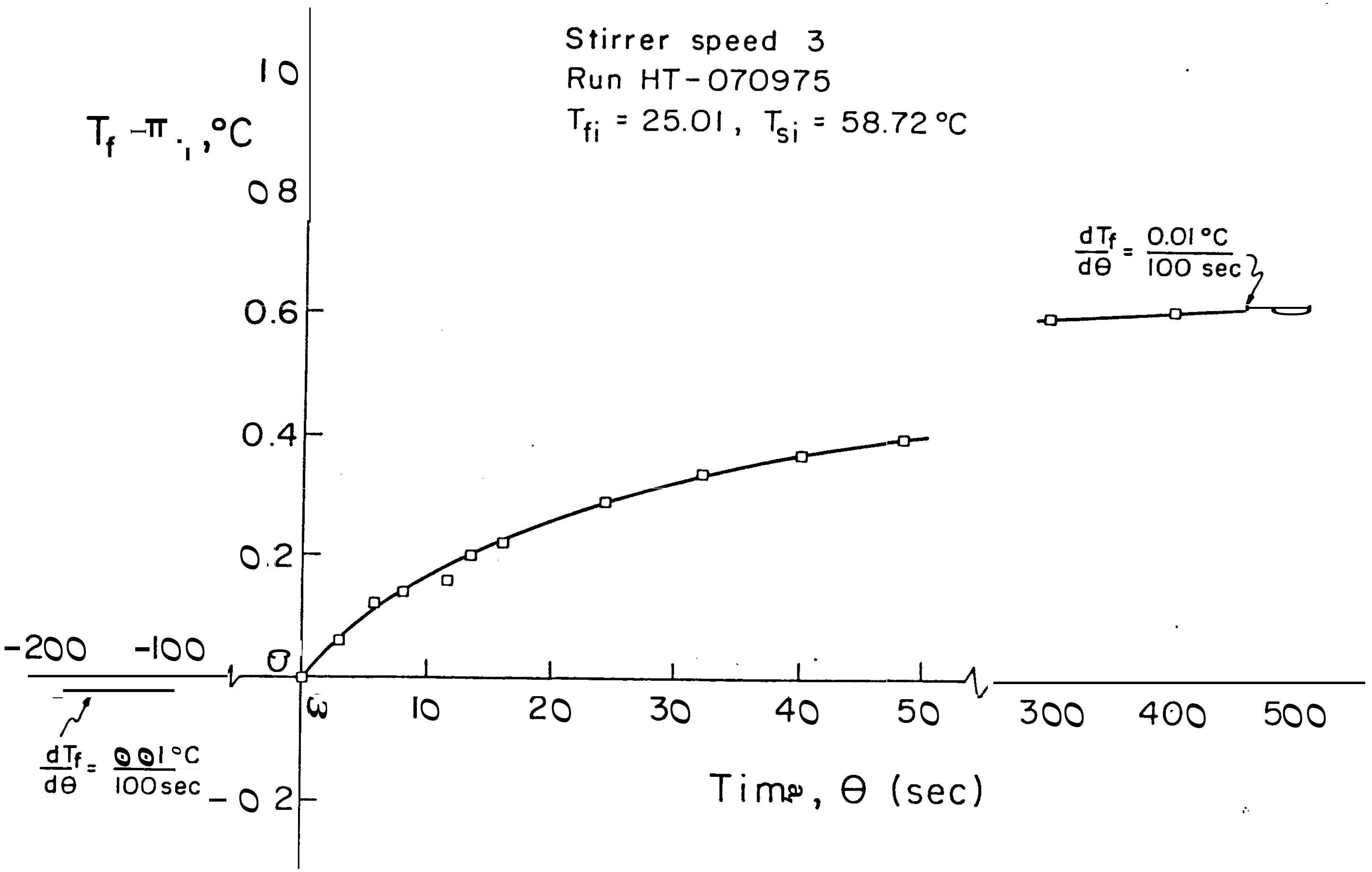

Figure 3 6 Heat transfer experiment data for Run HT-070975 is introduced and after equilibrium state is reached of about 0.01°C per 100 sec, which is used to correct the recorded temperature of the surrounding fluid. This rate of temperature increase is due to the combined effects of stirrer and environment conditions. It is noted that the stirrer speed has a negligible effect on the rate of temperature increase. The uncertainty of each temperature measurement is estimated at 0.01°C.

Experimental data for the cooling-down experiments are shown in Figs. 3.7 through 3.10 and are matched with the lumped-parameter model given in Chapter 2, Eq. (2.2). The heat transfer parameters for this system have been estimated from the slopes of straight lines in Figs. 3.7 through 3.10 and are listed in Tables 3.1 and 3.2. Table 3.1, Figs. 3.7 and 3.8 arc for the system with water in the cylinder jacket, while Table 3.2, Figs. 3.9 and 3.10 are for the system with air in the jacket of the cylinder.

For this study, heat transient experiments of spheres have been conducted in the system without water in the jacket. For a mean heat transfer coefficient, hA = 0.576 Btu/hr°F, the heat loss of the system to the surrounding fluid is estimated to be 0.0576 Btu for the experimental period of 360 sec, and a temperature difference of 1°F between the surrounding fluid and the system was noted. The heat transferred from the hot porous sphere to the surrounding fluid for the experimental period of 360 sec is estimated to be 3.0 Btu. The heat loss of the system, 0.0576 Btu, is negligible as compared to 3.0 Btu. Thus, the system is well insulated for the purpose of this experimental study.

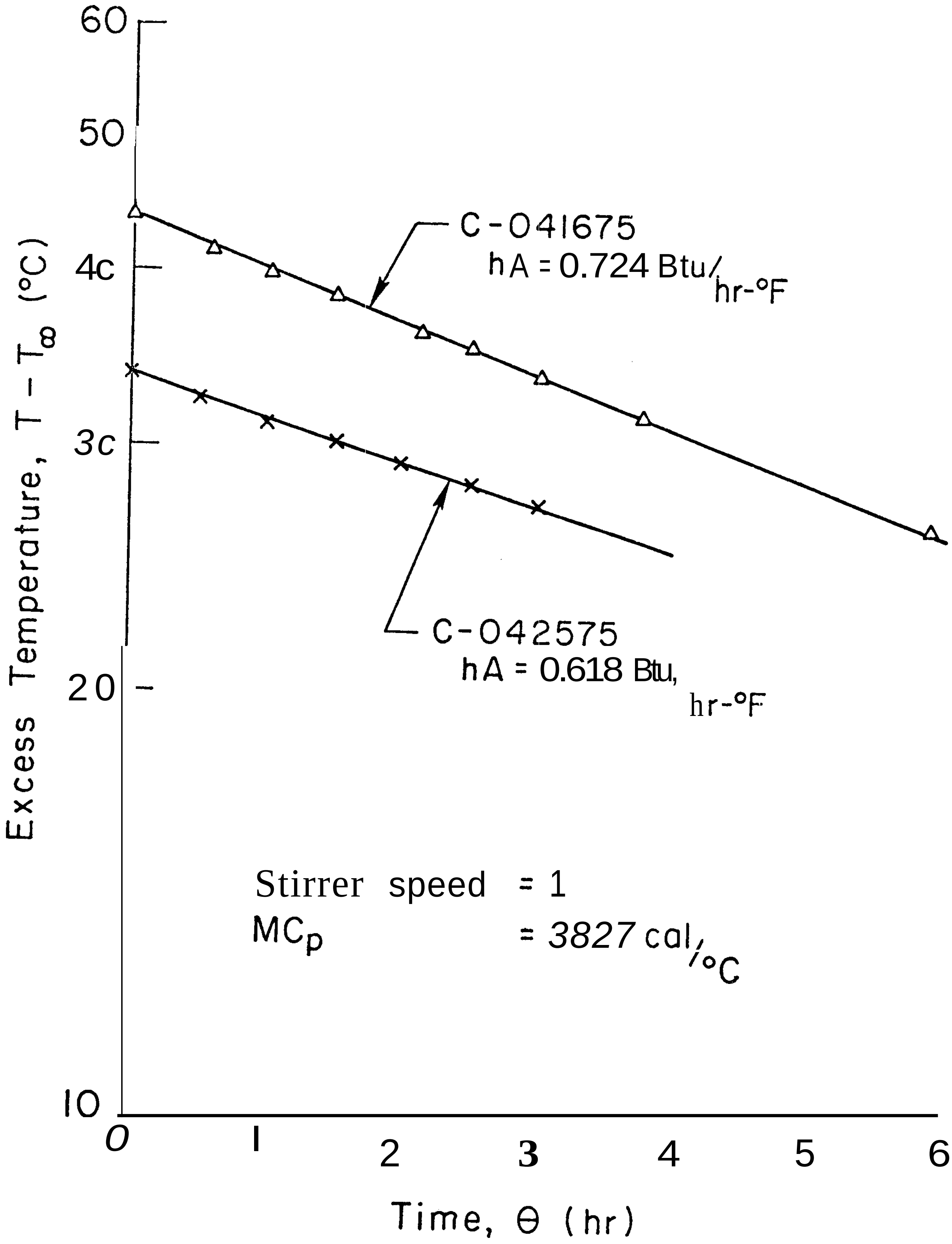

Figure 3.7 **Cool-down** experiment data for Runs C-041675 and *C-042575*

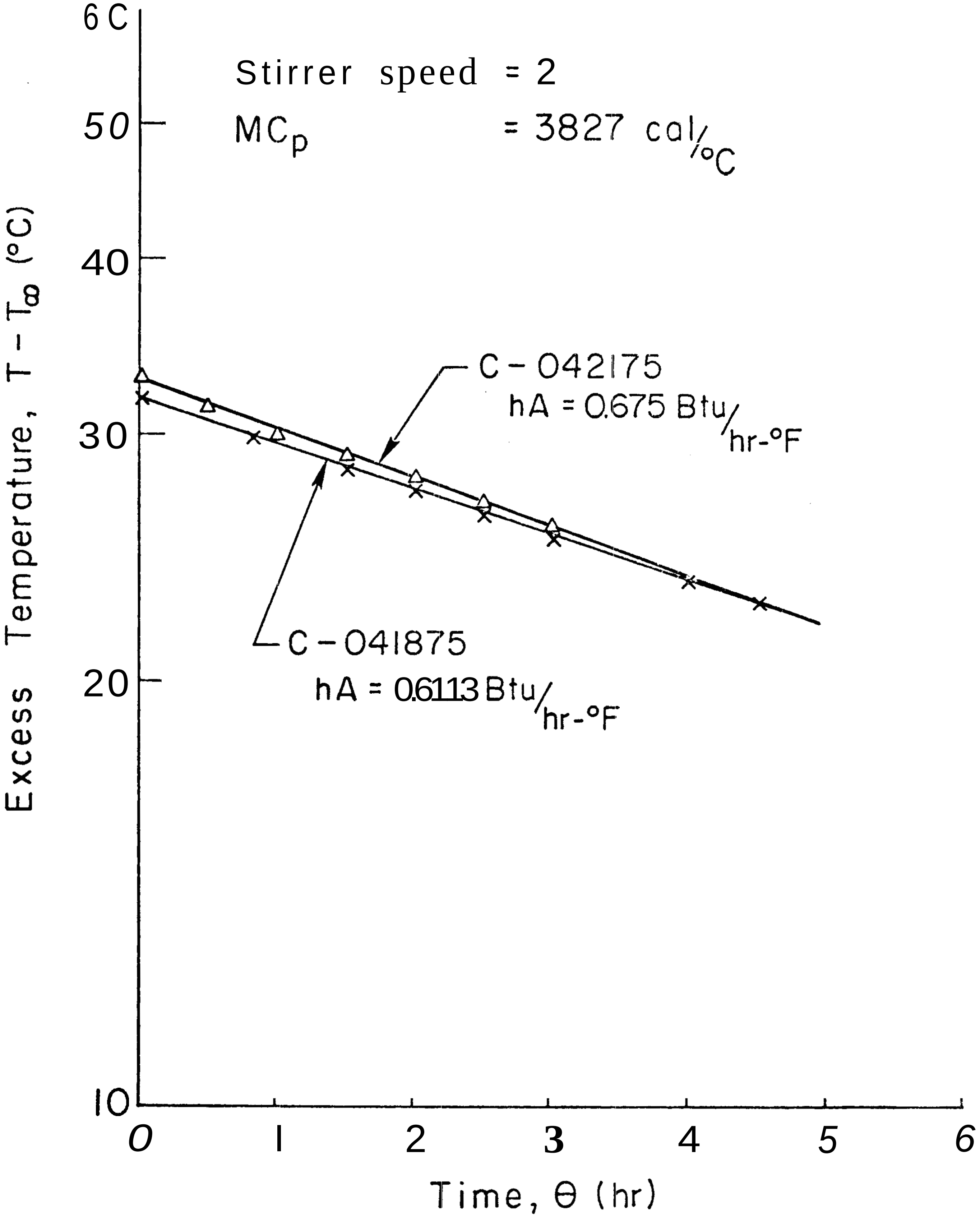

Figure 3.8 Cool-down! experiment data for Runs C-04187.5 and C-042175

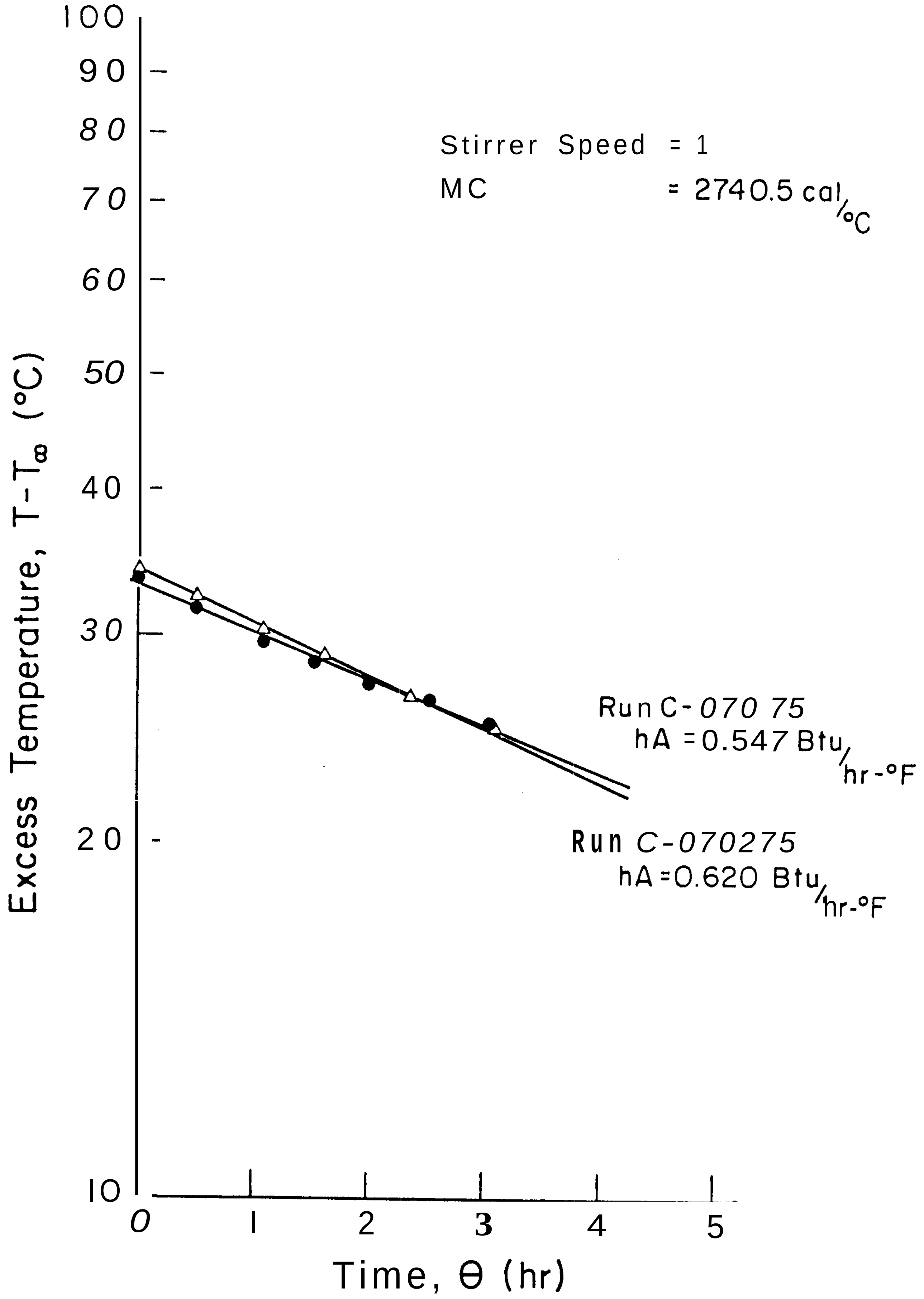

Figure 3.9 Cool-down experiment data for Runs C-070175 and C-070275

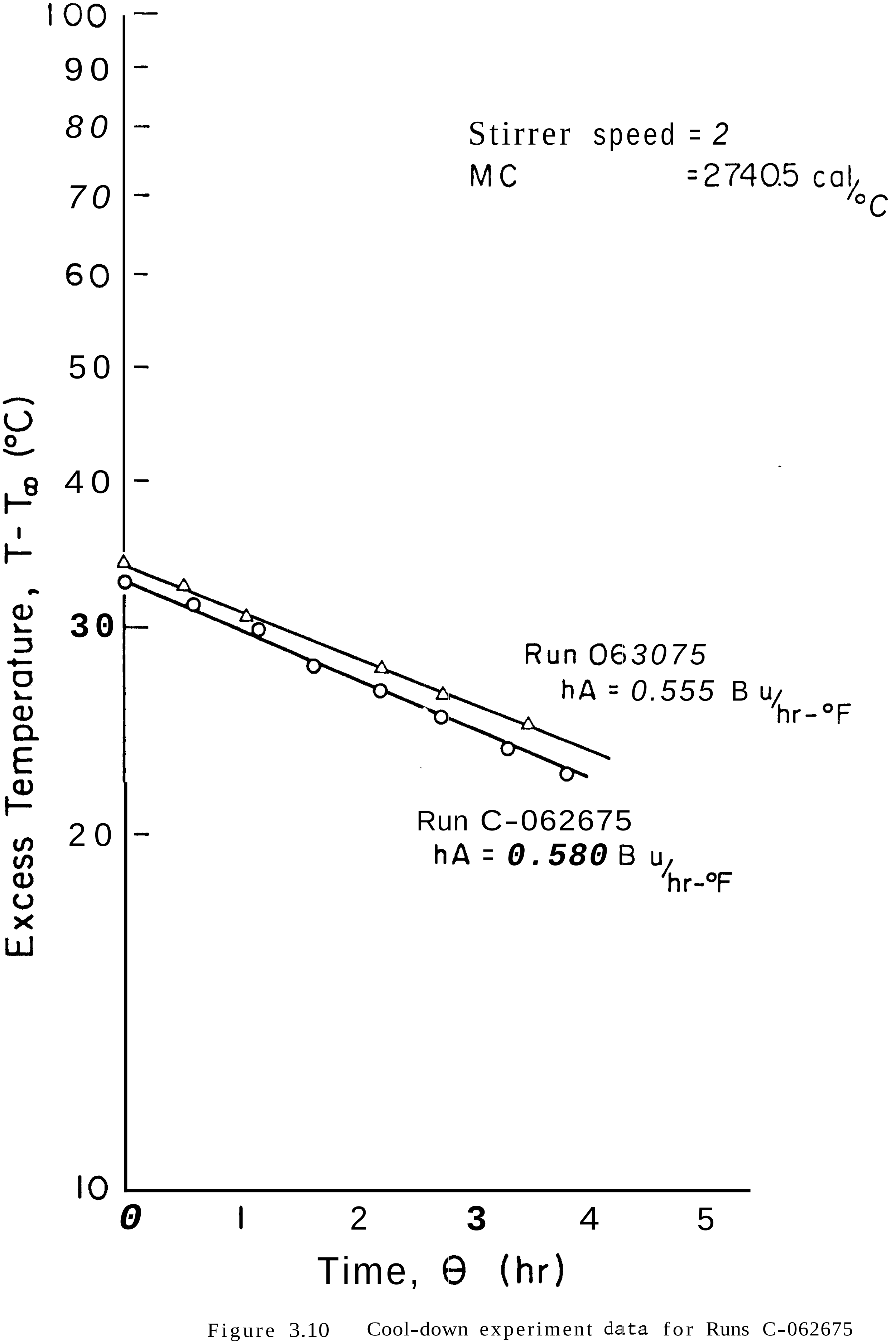

Figure 3.10 Cool-down experiment data for Runs C-062675 and C-063075

TABLE 3.1

Summary of Data from Cooldown Experiments*

| Run ID No. | Stirrer Speed | Total System Seat Capacity, MC(Btu/°F) | Measured Slope $hr^{-1}$ | Time Constant (hr) | Computed hA (Btu/hr °F) |
|---|---|---|---|---|---|
| C-041675 | 1 | 8.44 | - 0.0858 | 11.66 | 0.724 |
| C-042575 | 1 | 8.44 | - 0.0732 | 13.66 | 0.618 |
| C-041875 | 2 | 8.44 | - 0.0726 | 13.77 | 0.613 |
| C-042175 | 2 | 8.44 | - 0.0800 | 12.50 | 0.675 |

with water in cylinder jacket.

Mean = 0.658 Btu/hr °F

Standard Deviation = ± 0.053 Btu/hr °F

TABLE 3.2

Summary of Data from Cooldown Experiments"

| Run ID No. | Stirrer Speed | Total System Heat Capacity, MC(Btu/°F) | Measured Slope $hr^{-1}$ | Time Constant (hr) | Computed hA (Btu/hr °F) |
|---|---|---|---|---|---|
| C-070175 | 1 | 6.04 | - 0.0906 | 11.04 | 0.547 |
| C-070275 | 1 | 6.04 | - 0.1027 | 9.74 | 0.620 |
| C-062675 | 2 | 6.04 | - 0.0960 | 10.42 | 0.580 |
| C-063075 | 2 | 6.04 | - 0.0919 | 10.88 | 0.555 |

*without water in cylinder jacket.

Mean = 0.576 Btu/hr °F

Standard Deviation = ± 0.033 Btu/hr °F

# CHAPTER 4

# MATHEMATICAL MODELS FOR EXPERIMENTAL SYSTEMS

## 4.1 Mass Transfer Models

Figure 4.1 shows the schematic diagram of the mass transfer experimental setup. Mathematical models are designed to represent this physical system. A pseudo steady state model and a parametric model are presented in the following two subsections.

### 4.1.1 Pseudo Steady State Model

Figure 4.2 represents a time sequence of' a simple model of diffusion of tritiated water from a single rock into a surrounding fluid. An effective core of radius $r_c$ is used to denote the average spherical region into which the external water front has not yet diffused, so that the initial concentration of tritiated water within the core $C_c$, remains constant. Figure 4.2(a) shows the concentration profile in a rock initially saturated with $N_i$ molecules of HTO in the surrounding fluid of external water. Figure 4.2(b) represents the concentration profile in the partially diffused rock at time $t$. Figure 4.2(c) exhibits the completely-diffused rock after an infinite time.

The mathematical results of the front model can be summarized as

$$D_e = \frac{C_c R^2 [1 - 3(\frac{r_c}{R})^2 + 2(\frac{r_c}{R})^3]}{6 \phi \int_0^t (C_c - C_f)\, dt} , \tag{4.1}$$

$$[\tfrac{2}{3} \pi R \phi (C_c - C_f)] r_c^2 + [\tfrac{2}{3} \pi R^2 \phi (C_c - C_f)] r_c + [C_f V - \tfrac{4}{3} \pi R^3 \phi (C_c - C_f)] = 0 . \tag{4.2}$$

Equation (4.2) relates the measurable quantities, $C_c$, $C_f$, $R$, $\phi$,

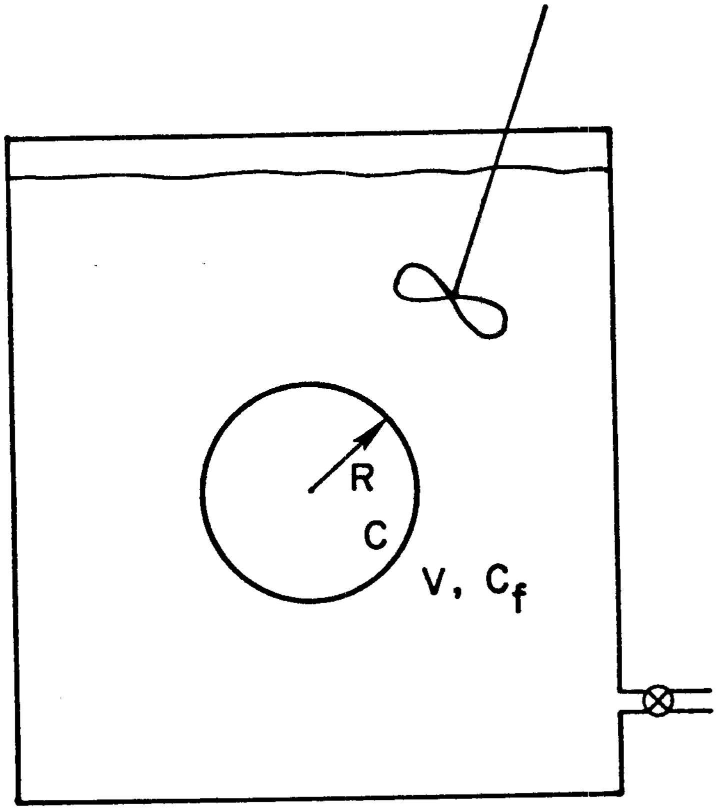

Figure 4.1 Schematic diagram of mass transfer experiment setup

$r$ = distance from center of rock

$R$ = radius of rock

$r_c$ = radius of core

$C$ = concentration of tritiated water of any radius $r$

$C_c$ = concentration of tritiated water in core

$C_b$ = concentration of tritiated water in surrounding fluid

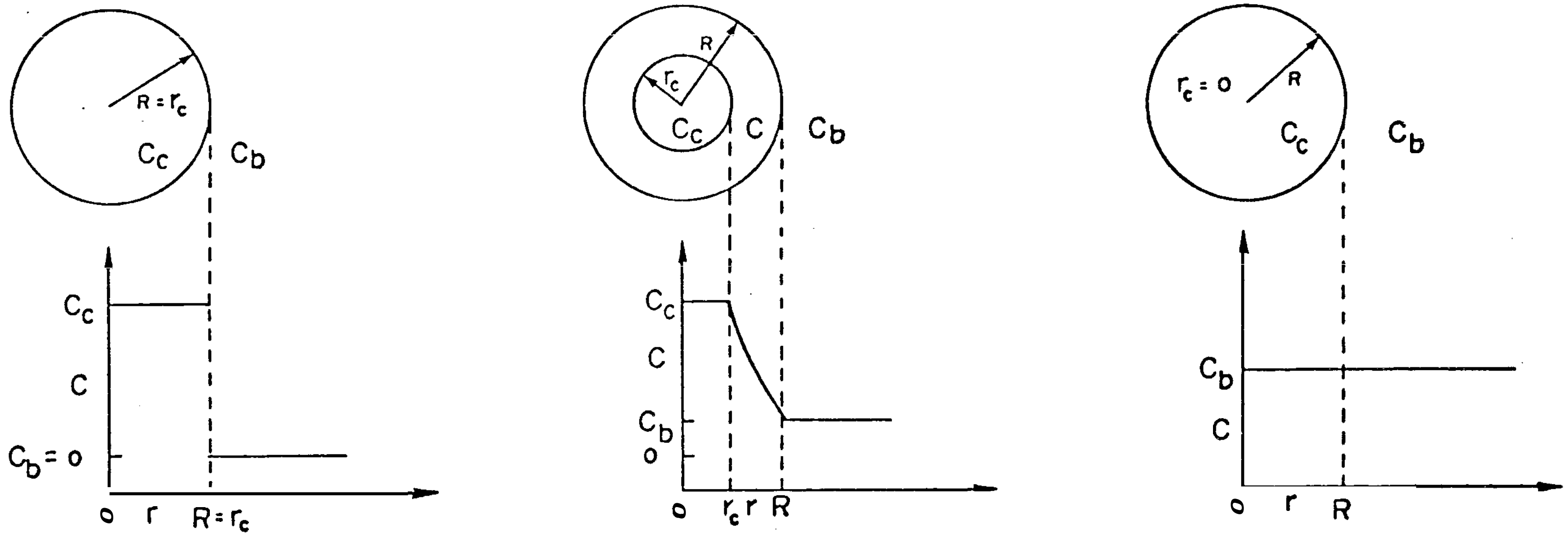

(a) $t = 0$ (b) $t$ (c) $t \to \infty$

Figure 4.2 Representation of front model in the sequence of time and V, to the effective core radius $r_c$ for the front model. The effective diffusivity, $D_e$, can be calculated from Eqs. (4.1) and (4.2) from the known values of $R$, $\phi$, $V$, $C_c$ and the measured values of $C_f$, as a function of time. The derivation of this model is given in Appendix A.

### 4.1.2 Parametric Model without. Skin Effect

In this model a system as the one depicted in Fig. 4.1 is considered. The system consists of two parts, a porous sphere, the void space of which is filled with a solution of tritiated water, and a surrounding fluid which is considered to have a uniform concentration. The system is subject to the following conditions:

1. The initial concentration of tritiated water in the porous sphere is uniform.
2. The outside solution always has a uniform concentration and is equal to the surface concentration of the porous sphere.
3. The matrix of the porous sphere is inert.
4. The disintegration of tritiated water is negligible due to the long half-life of tritium, 12.4 years.

A mass balance on the tritiated water in the sphere leads to the following partial differential equation:

$$\frac{\delta C_s}{\delta \theta} = D_e \frac{1}{r^2} \frac{\delta}{\delta r}\left(r^2 \frac{\delta C_s}{\delta r}\right), \qquad (4.3)$$

where

$C_s$ = the concentration of tritiated water,

$D_e$ = the effective diffusion coefficient of tritiated water,

$\theta$ = time, and

$r$ = the distance from the center of the porous sphere.

A mass balance at the interface of the two parts gives:

$$V \frac{dC_f}{d\theta} = - D_e \left. \frac{\delta C_s}{\delta r} \right|_{r=R} A\phi \ , \tag{4.4}$$

where

$R$ = the radius of the sphere,

$A$ = the surface area of the sphere, i.e. $4\pi R^2$ ,

$C_f$ = the concentration of tritiated water in the surrounding fluid,

$\phi$ = the porosity of the sphere, and

$V$ = the volume of the surrounding fluid.

The initial and boundary conditions are as follows:

1. The concentration within the porous sphere and that in the surrounding fluid are initially $C_i$ and $C_{fi}$ , respectively, that is, when $\theta = 0$ ,

$$C_s = C_{si} \ , \quad \text{for} \quad r \leq R \ ,$$

$$C_f = C_{fi} \ , \quad \text{for} \quad r > R \ .$$

2. At the interface between the sphere and the surrounding fluid, the concentration is continuous, that is, at $r = R$ ,

$$C_s = C_f \ , \quad \text{for} \quad t > 0 \ .$$

For simplicity, the following set of dimensionless quantities is introduced:

$$X = \frac{C_s - C_{si}}{C_{fi} - C_{si}} ,$$

$$Y = \frac{C_f - C_{si}}{C_{fi} - C_{si}} ,$$

$$\theta^* = \frac{D_e \theta}{R^2} , \qquad (4.5)$$

$$r^* = r/R ,$$

$$\omega = \frac{RA\phi}{3V} = \frac{4\pi R^3 \phi}{3V} .$$

Substituting **Eq.** (4.5) into **Eqs.** ***(4.3)*** and (4.4) gives

$$\frac{\delta X}{\delta \theta^*} = \frac{1}{r^{*2}} \frac{\delta}{\delta r^*} \left(r^{*2} \frac{\delta X}{\delta r^*}\right) , \qquad (4.6)$$

$$\frac{dY}{d\theta^*} = - 3\omega \left.\frac{\delta X}{\delta r^*}\right|_{r^*=1} . \qquad (4.7)$$

The initial and boundary conditions become:

1. When $\theta^* = 0$ ,

$$X = 0 ,$$

$$Y = 1 .$$

2. At $r^* = 1$ ,

$$X = Y , \quad \text{for} \quad \theta^* > 0 ,$$

3. At $r^* = 0$ ,

$$Z = 0 , \quad \text{for} \quad \theta^* > 0 .$$

The analytical solution for the system equations ***(4.6)*** and (4.7), subject to the above initial and boundary conditions, has been obtained (Carslaw and Jeager, 1959; Crank, 1956):

$$X(\theta^*,r^*) = \frac{1}{\omega + 1} + \frac{2}{r^*} \sum_{n=1}^{\infty} \frac{\sin(\gamma_n r^*)}{\sin(\gamma_n)} \quad \frac{e^{-\gamma_n^2 \theta^*}}{[(3\omega + 3) + \frac{\gamma_n^2}{3\omega}]} , \tag{4.8}$$

$$Y(\theta^*) = \frac{1}{\omega + 1} + 2 \sum_{n=1}^{\infty} \frac{e^{-\gamma_n^2 \theta^*}}{[(3\omega + 3) + \frac{\gamma_n^2}{3\omega}]} , \tag{4.9}$$

where $\gamma_n$ satisfies

$$\gamma \cot \gamma = 1 + \frac{\gamma^2}{3\omega} .$$

Detailed derivations through the use of Laplace transforms are given in Appendix B.

It is convenient to define a dimensionless variable, $C_f^*$ , whose value ranges from 0 to 1 :

$$C_f^* = \frac{C_f - C_{fi}}{C_{f\infty} - C_{fi}} .$$

$C_f^*$ is related to $Y$ by

$$C_f^* (\theta^*) = \frac{(1 + \omega)}{\omega} (1 - Y(\theta^*)) .$$

Substituting Eq. (4.9) into the above equation yields

$$C_f^* = 1 - 2 \frac{1+\omega}{\omega} \sum_{n=1}^{\infty} \frac{e^{-\gamma_n^2 \theta^*}}{[(3\omega + 3) + \frac{\gamma_n^2}{3\omega}]} \tag{4.10}$$

Figure 4.3 shows $C_f^*$ vs $\theta^*$ with $\omega$ as parameter. As can be seen, the curve with $\omega \to 0$ can represent the range $0 < W < 0.1$ well.

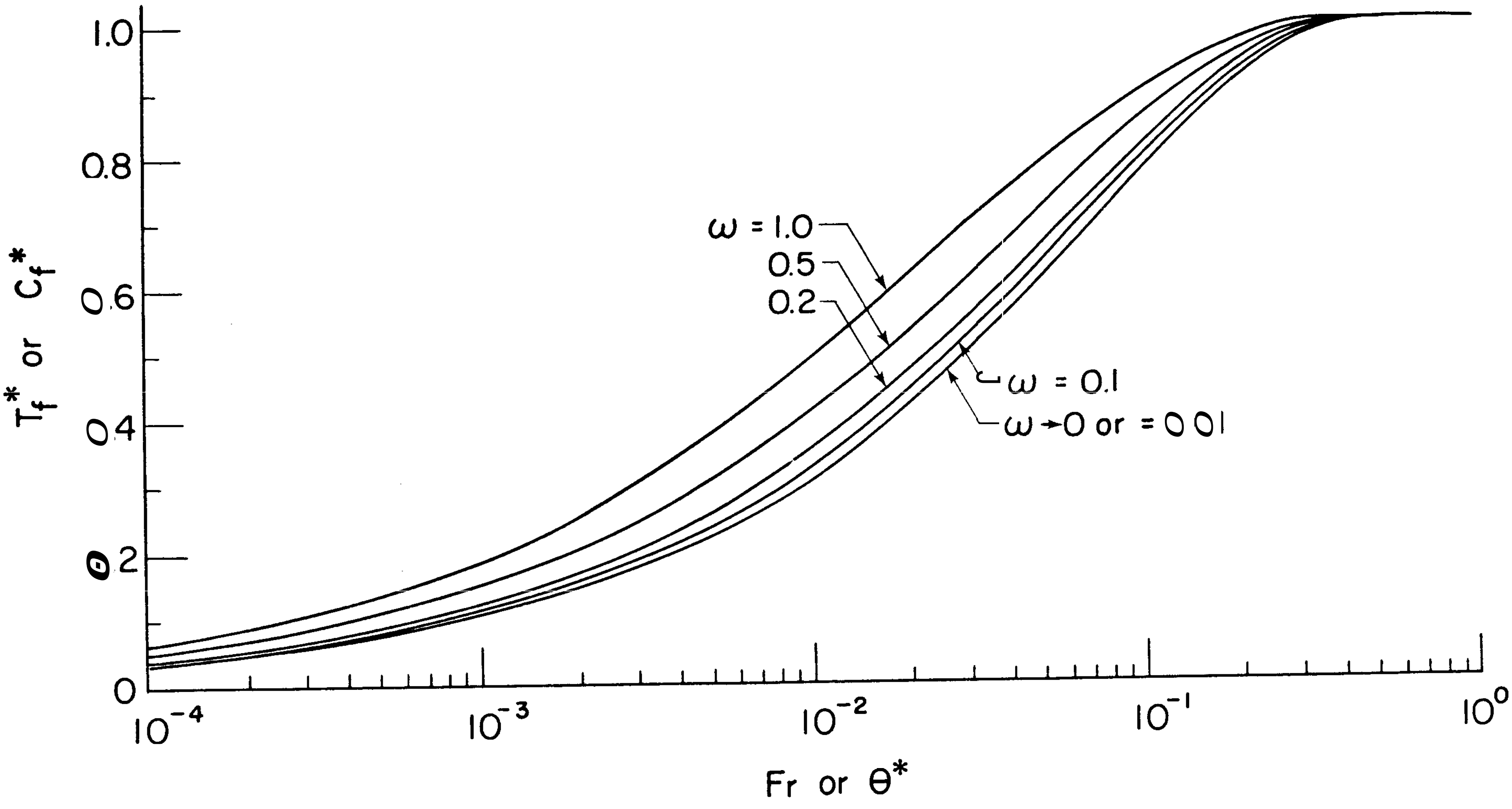

Figure 4.3 Results of parametric model with capacity ratio, ω, as parameter

Figure 4.4 presents $C_f^*$ vs $\theta^*$ with $\omega \rightarrow 0$ on the log-log scale; the line can represent the range $0 < \omega < 0.1$ within the accuracy of 2% for $C_f^*$ .

## 4.2 Heat Transfer Models

Figure 4.5 shows the schematic diagram of the heat transfer setup. The system is insulated from the environment:. Mathematical models designed to represent this physical system include the one lump model and the parametric model.

### 4.2.1 One Lump Model

In the One Lump Model, the temperature inside the sphere is assumed to be uniform. This is consistent with the fact that the internal resistance to heat transfer is assumed to be negligible compared to the interface resistance.

The rate equation for heat transfer from the sphere to the water can be expressed as

$$q = hA(T_s - T_f) \quad . \tag{4.11}$$

The energy balance for the water can be written as

$$C_w \frac{dT_f}{d\theta} = q \quad . \tag{4.12}$$

Combination of the energy balance equation, Eq. (4.11), and the rate equation, Eq. (4.12), results in

$$C_w \frac{dT_f}{d\theta} = hA(T_s - T_f) \quad , \tag{4.13}$$

where

$C_w$ = the heat capacity of the water,

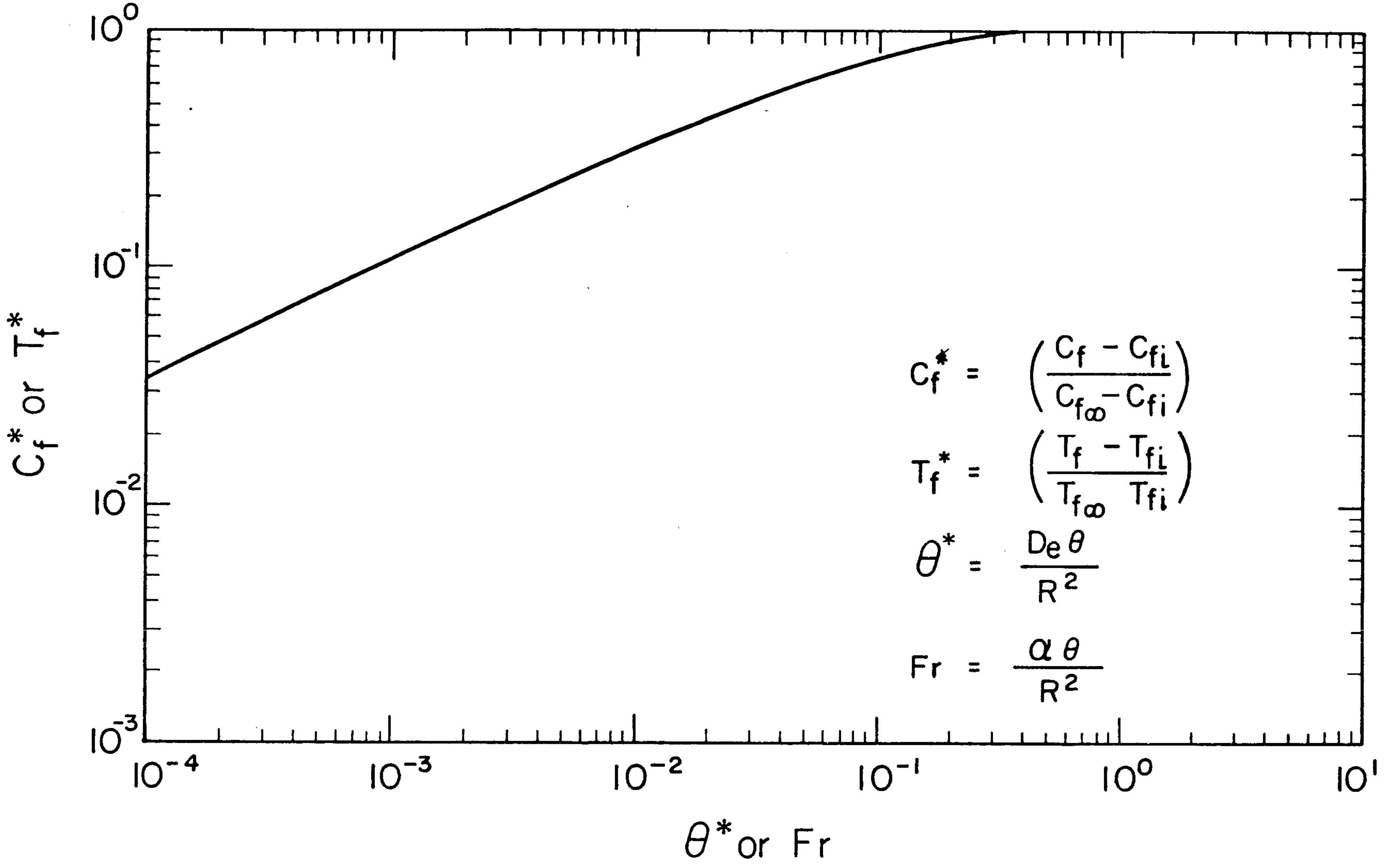

Figure 4.4 Results of parametric model on log-log paper for $\omega \to 0$

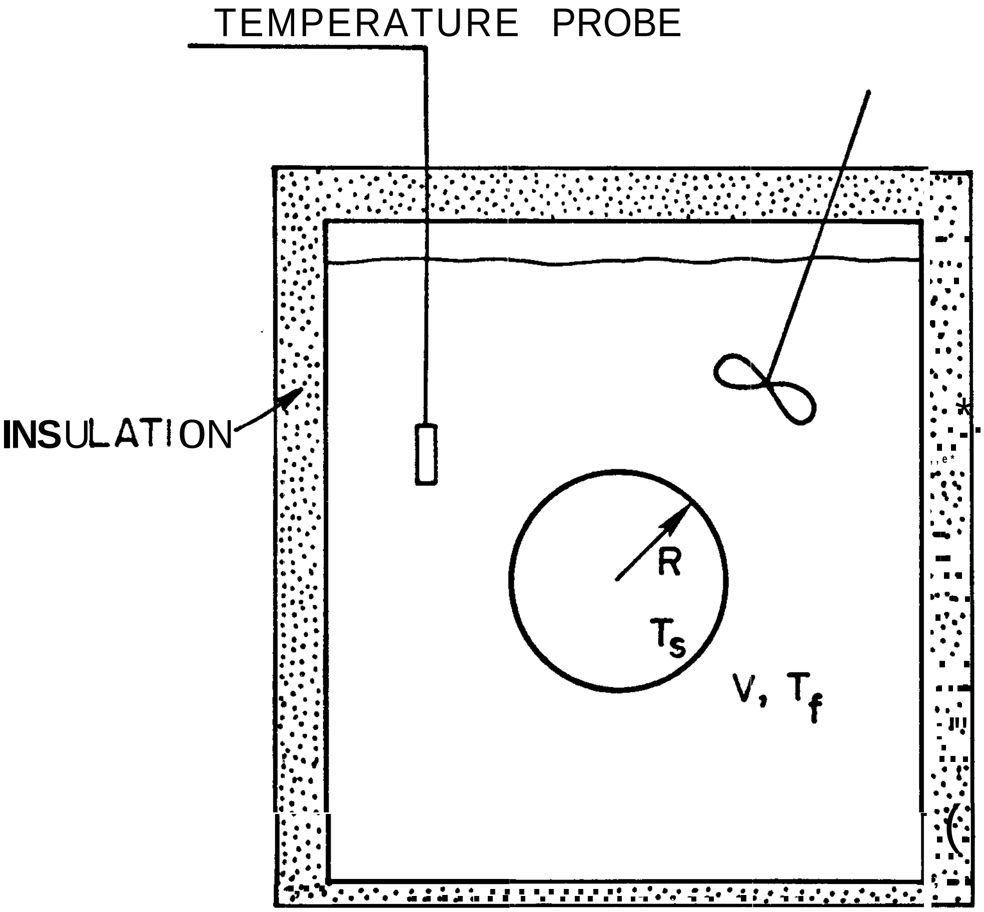

Figure 4.5 Schematic diagram of heat transfer experiment setup

$T_f$ = the temperature of the water,

$T_{fi}$ = the initial temperature of the water,

$T_s$ = the temperature of the sphere,

$hA$ = the heat transfer parameter, and

$\theta$ = time.

Assuming that the experimental system is isolated from the surrounding fluid, the following equation is obtained:

$$C_w(T_f - T_{fi}) = C_s(T_{si} - T_s) \ , \tag{4.14}$$

where $C_s$ = the heat: capacity of the sphere, and $T_{si}$ = the initial temperature of the sphere. From Eq. (4.14),

$$T_s = \frac{C_w}{C_s} (T_f - T_{fi}) + T_{si} \ .$$

Let $1/\omega = C_w/C_s$, and thus,

$$T_s = - \frac{1}{\omega}(T_f - T_{fi}) + T_{si} \ . \tag{4.15}$$

Substituting Eq. (4.15) into **(4.13)** yields

$$C_w \frac{dT_f}{d\theta} = hA(T_{si} - \frac{1}{\omega} (T_f - T_{fi}) - T_f) \ . \tag{4.16}$$

Rearranging Eq. *(4.16)* yields

$$C_w \frac{d(T_f - T_{fi})}{d\theta} = - hA(\frac{1}{\omega} + 1) (T_f - T_{fi}) + hA(T_{si} - T_{fi}) \ . \tag{4.17}$$

Let

$$\tilde{T}_f^* = \frac{T_f - T_{fi}}{T_{si} - T_{fi}}$$

and **Eq.** (4.17) becomes

$$\frac{d\tilde{T}_f^*}{d\theta} + \frac{hA(1/\omega + 1)}{C_w}\tilde{T}_f^* = \frac{hA}{C_w} \quad . \tag{4.18}$$

Let $\theta^* = hA\theta/C_w$ , and Eq. (4.18) becomes

$$\frac{d\tilde{T}_f^*}{d\theta^*} + (\frac{1}{\omega} + 1)\,\tilde{T}_f^* = 1 \quad , \tag{4.19}$$

subject to $\tilde{T}_f^* = 0$ , at $\theta^* = 0$ .

Solving Eq. (4.19) with the above initial condition yields

$$\tilde{T}_f^* = \frac{1}{1/\omega + 1}\,(1 - e^{-(1/\omega + 1)\,\theta^*}) \quad ,$$

or

$$\ln\left\{1 - (\frac{1}{\omega} + 1)\,\tilde{T}_f^*\right\} = -\,(\frac{1}{\omega} + 1)\,\theta^* \quad . \tag{4.20}$$

For $1/\omega >> 1$ , **Eq.** (4.20) can be simplified as

$$\ln[1 - (\frac{1}{\omega} + 1)\,\tilde{T}_f^*] \simeq -\frac{hA}{C_s}\,\theta \quad . \tag{4.21}$$

This model predicts a linear relationship between $\ln[1 - (1/\omega + 1)\,\tilde{T}_f^*]$ and $\theta$ . If the model is adequate for the system, the experimental data should behave semi-log linearly, and vice versa.

### 4.2.2 Parametric Model without Skin Effect

In this model a solid sphere of uniform initial temperature is cooled in a finite mass of fluid, well stirred and externally insulated. The surface temperature of the sphere is assumed equal at all subsequent times to that of the fluid, which is so well stirred that its temperature is always uniform throughout and is: equal to the surface temperature of the sphere.

An energy balance in the sphere leads to the following partial differential equation:

$$\frac{\partial T_s}{\partial \theta} = \alpha \frac{1}{r^2} \frac{\partial}{\partial r} \left(r^2 \frac{\partial T_s}{\partial r}\right) , \tag{4.22}$$

where

$T_s$ = temperature,

$\alpha$ = the thermal diffusivity of the sphere,

0 = time, and

r = the distance from the center of the sphere.

An energy balance at the interface of the sphere and the surrounding fluid gives

$$(\rho C_p V)_{\text{fluid}} \frac{dT_f}{d\theta} = - \alpha (\rho C_p)_{\text{sphere}} \, 4\pi R^2 \left. \frac{\partial T_s}{\partial r} \right|_{r=R} ,$$

that is,

$$C_f \frac{dT_f}{d\theta} = - \frac{3\alpha}{R} C_s \left. \frac{\partial T_s}{\partial r} \right|_{r=R} , \tag{4.23}$$

where

$C_f = (\rho C_p V)_{\text{fluid}}$ = the heat capacity of the surrounding fluid,

$C_s = (\rho C_p)_{\text{sphere}} \, 4/3 \, \pi R^3$ = the heat capacity of the sphere,

R = the radius of the sphere,

$T_f$ = the temperature in the surrounding fluid, and

V = the volume of the surrounding fluid.

The initial and boundary conditions are as follows:

1. The temperature within the sphere and that in the surrounding fluid are initially $T_{si}$ and $T_{fi}$, respectively, that is, when $\theta = 0$,

$$T_s = T_{si} \;, \text{ for } r \leq R \;,$$

$$T_f = T_{fi} \;, \text{ for } r > R \;.$$

2. At the interface between the sphere and the surrounding fluid, the temperature is continuous, that is, at $r = R$,

$$T_s = T_f \;, \quad \text{for } \theta > 0 \;.$$

For simplicity, the following set of dimensionless quantities is introduced:

$$X = \frac{T_s - T_{si}}{T_{fi} - T_{si}} \;,$$

$$Y = \frac{T_f - T_{si}}{T_{fi} - T_{si}} \;,$$

$$\theta^* = \frac{\alpha\theta}{R^2} \;, \tag{4.24}$$

$$r^* = \frac{r}{R} \;,$$

$$\omega = \frac{C_s}{C_f} \;.$$

Substituting Eq. (4.24) into Eqs. (4.22) and (4.23) gives

$$\frac{\delta X}{\delta \theta^*} = \frac{1}{r^{*2}} \frac{\delta}{\delta r^*} \left(r^{*2} \frac{\delta X}{\delta r^*}\right) \;, \tag{4.25}$$

$$\frac{dY}{d\theta^*} = -\, 3\omega \left.\frac{\delta X}{\delta r^*}\right|_{r^*=1} \;. \tag{4.26}$$

The initial and boundary conditions become:

1. When $\theta^* = 0$ ,

$$X = 0 \ ,$$

$$Y = 0 \ .$$

2. At $r^* = 1$ ,

$$X = Y \ , \quad \text{for} \quad \theta > 0 \ .$$

The analytical solution for system equations *(4.25)* and (4.26), subject to the above initial and boundary conditions has been obtained (Carslaw and Jeager, 1959; Crank, 1956):

$$X(\theta^*,r^*) = \frac{1}{\omega + 1} + \frac{2}{r^*} \sum_{n=1}^{\infty} \frac{\sin(\gamma_n r^*)}{\sin(\gamma_n)} \frac{e^{-\gamma_n^2 \theta^*}}{[3(\omega + 1) + \frac{\gamma_n^2}{3\omega}]} \ , \qquad (4.27)$$

$$Y(\theta^*) = \frac{1}{\omega + 1} + 2 \sum_{n=1}^{\infty} \frac{e^{-\gamma_n^2 \theta^*}}{[3(\omega + 1) + \frac{\gamma_n^2}{3m}]} \ , \qquad (4.28)$$

where $\gamma_n$ satisfies

$$\gamma \cot \gamma = 1 + \frac{\gamma^2}{3w} \ .$$

Detailed derivations through the use of Laplace transforms are given in Appendix B.

**It** is convenient to define a dimensionless variable, $T_f^*$ , whose value ranges from 0 to 1 .

$$T_f^* = \frac{T_f - T_{fi}}{T_{f\infty} - T_{fi}} \ .$$

$T_f^*$ is related to Y by

$$T_f^*(\theta^*) = \frac{1+\omega}{\omega}(1 - Y(\theta^*)) .$$

Substituting Eq. (4.30) into the above equation yields

$$T_f^* = 1 - 2\,\frac{1+\omega}{\omega}\sum_{n=1}^{m}\frac{e^{-\gamma_n^2\theta^*}}{[(3\omega + 3) + \frac{\gamma_n^2}{3\omega}} . \qquad (4.29)$$

Equation (4.29) is similar to Eq. (4.10). Figure 4.4 presents $T_f^*$ vs $\theta^*$ on the log-log scale with $\omega \to 0$ ; the line can represent the range $0 < \omega < 0.1$ within the accuracy of 2% for $T_f^*$ .

## 4.3 Comparisons of Models

Two models have been proposed for a mass transfer experimental system, a pseudo steady state model and a parametric model without skin effect. Two models, a one lump model and a parametric model, have also been proposed for the heat transfer experimental system. Comparisons of the models are shown in Tables 4.1 and 4.2, respectively.

Figure 4.6 presents the simulation results of the two mass transfer models. The pseudo steady state model predicts lower values of Y , $(T_f - T_{si})/(T_{fi} - T_{si})$ , than those predicted by the parametric model, especially when the dimensionless time is large ( $> 10^{-2}$). Pseudo steady state assumption is not good when the core radius is small, or when the intermediate layer is thick.

TABLE 4.1

Comparisons of Mass Transfer Models

| Models: | Pseudo Steady State Model | Parametric Model without Skin Effect |
|---|---|---|
| Remarks: | Pseudo steady state is assumed.<br>Interface resistance is neglected. | Interface resistance is neglected. |

TABLE 4.2

Comparisons of Heat Transfer Models

| Models: | One Lump Model | Parametric Model without Skin Effect |
|---|---|---|
| Remarks: | Lntrasphere resistance is neglected. | Interface resistance is neglected. |

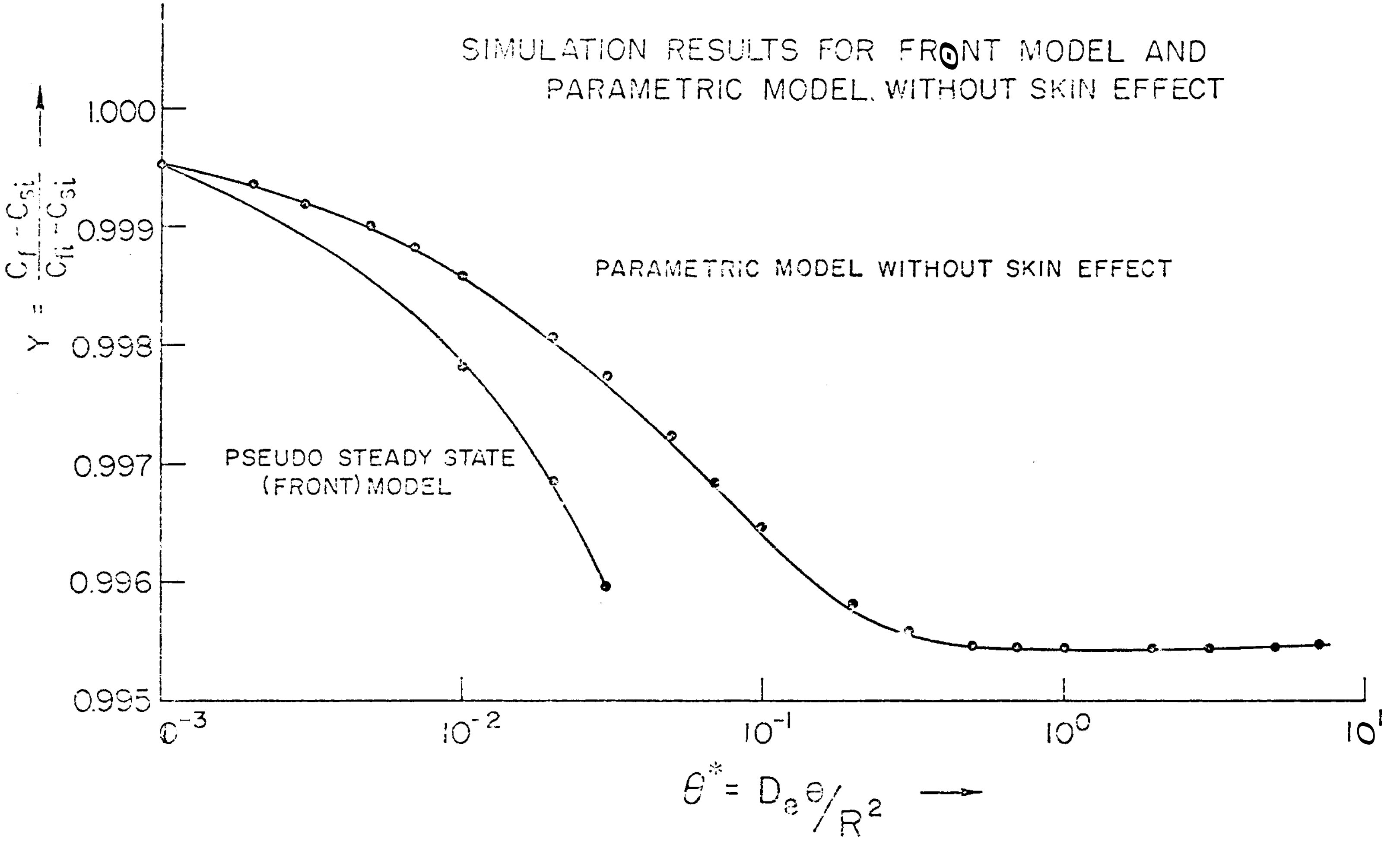

Figure 4.6 Comparison of simulation results for pseudo steady state model and parametric model

# CHAPTER 5

## ANALYSES OF EXPERIMENTAL RESULTS

### 5.1 Effective Diffusivity

The mass transfer experimental data have been matched with Fig. 4.5, developed in Chapter 4, to estimate the value of effective diffusivity. Experimental data were plotted as $C_f^*$ vs $\theta$ . Figure 4.5 related $C_f^*$ vs $\theta^*$ . The dimensionless time, $\theta^*$ , is related to real time, $\theta$ , by the following definition:

$$\theta^* = \frac{D_e \theta}{R^2} \; .$$

Taking the logs of both sides, we obtain

$$\log \theta^* = \log \theta + \log \frac{D_e}{R^2} \; .$$

For a given sphere, $D_e$ and $R$ are constants. Therefore, $\log \theta^*$ always differs from $\log \theta$ by a constant. The experimental data plotted on log-log paper can be shifted from left to right parallel at the top of Fig. 4.5 to get the best match. The effective diffusivity is calculated from the match point.

Figures 5.1, 5.2, and 5.3 show the results of this matching. As can be seen, the model without skin effect cannot fit the experimental data equally well in the whole range of time. Incorporating skin effect into the present model can improve the fit.

The effective diffusivity of tritiated water in the synthetic rock is found to increase with increasing porosity. Figure 5.4 shows the

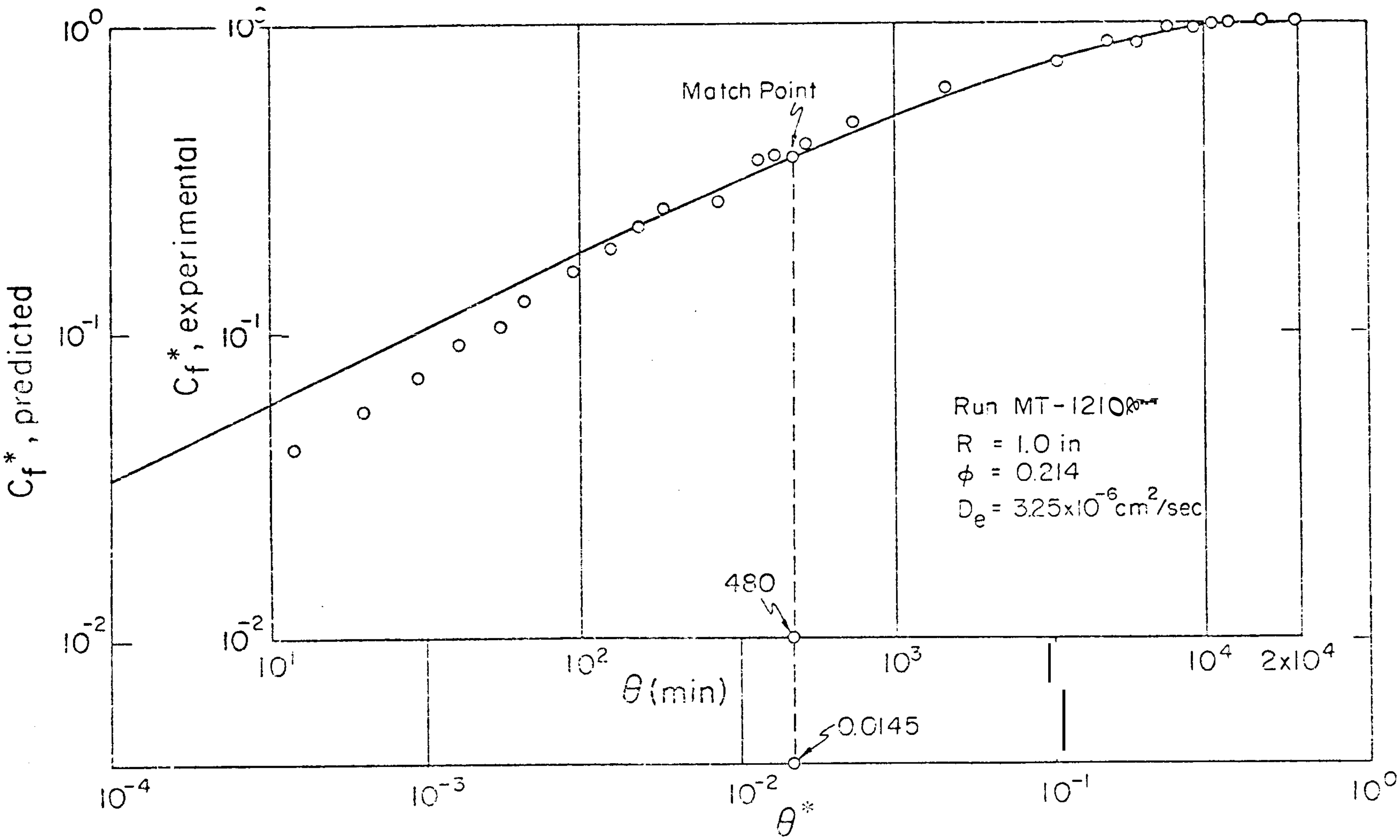

Figure 5.1 Type curve matching for Run MT-121074

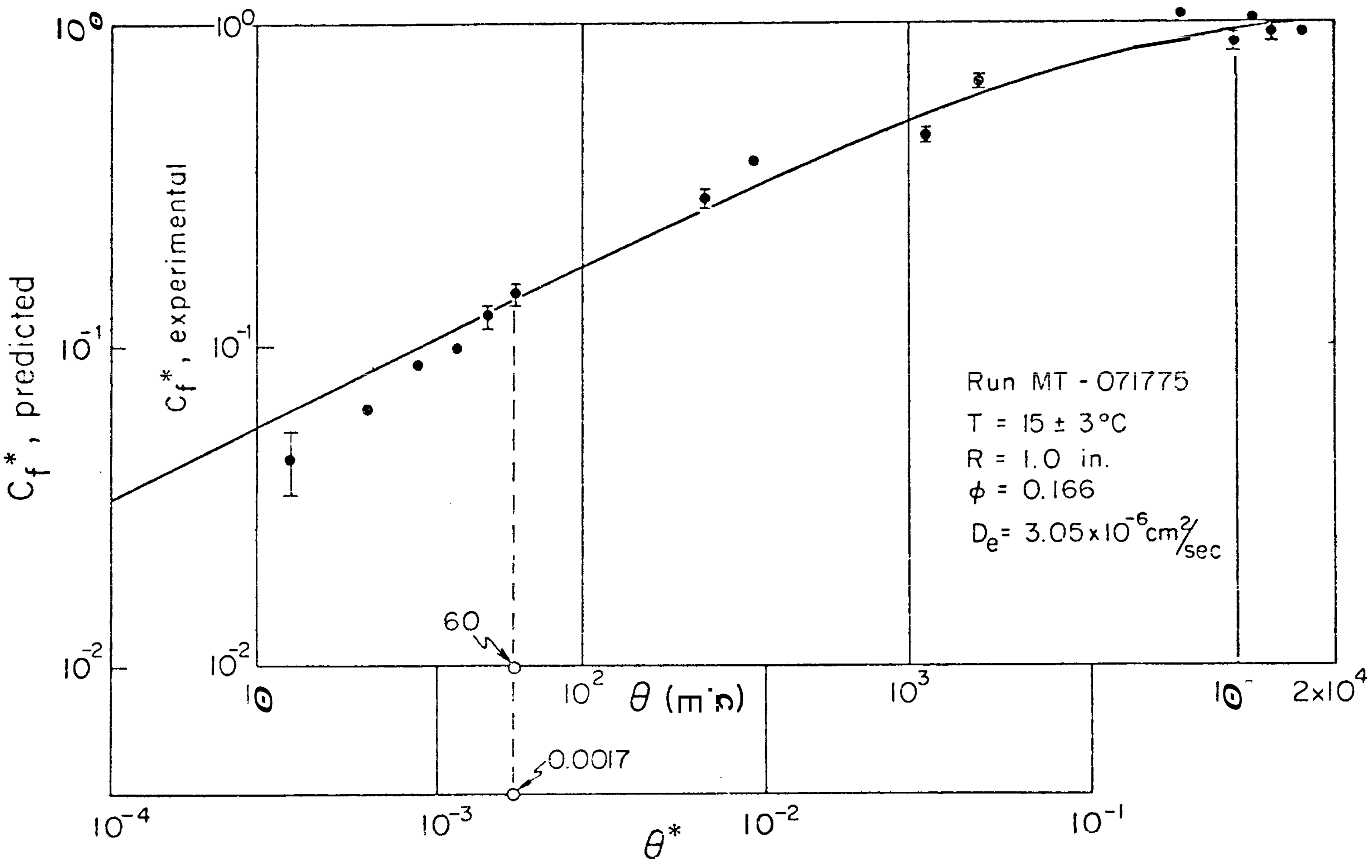

Figure 5.2 Type curve matching for Run MT-071775

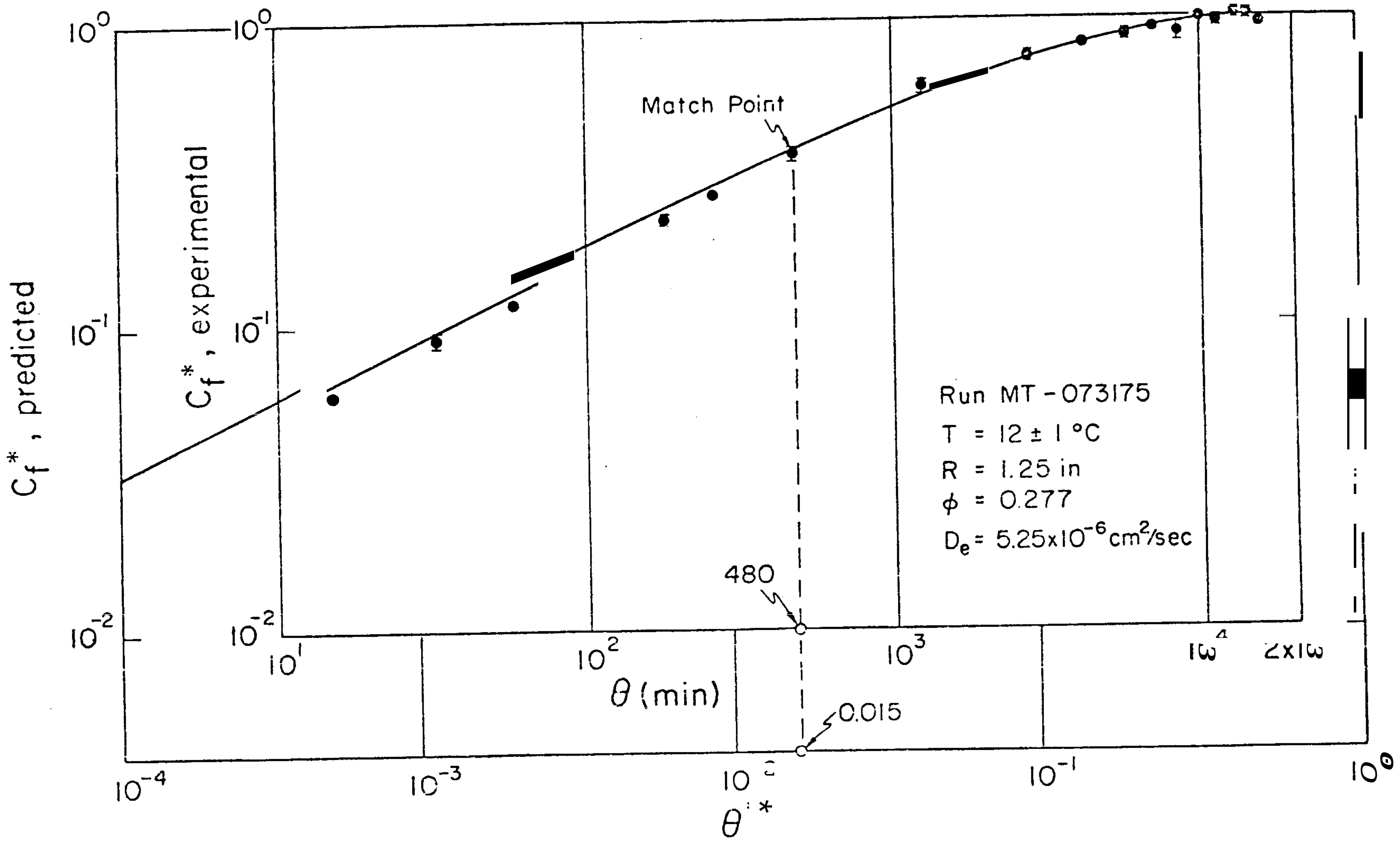

Figure 5.3 Type curve matching for Run MT-073175

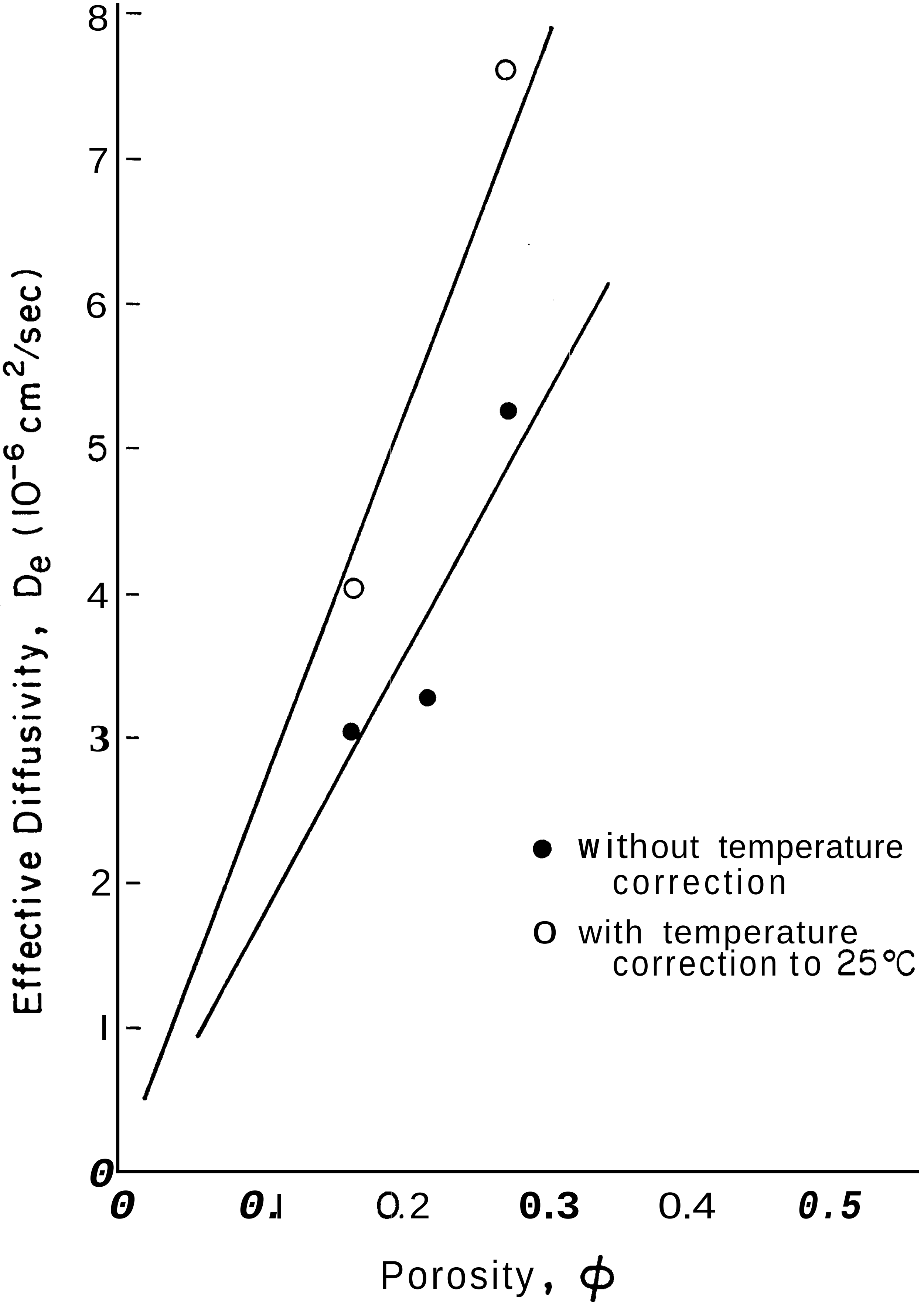

Figure 5.4 Correlation of effective diffusivity and porosity

relationship. The dark circle data are evaluated at different temperatures, and the open circle data are obtained through temperature correction to 25°C based on the work by Wang (1952). The following correlation for effective diffusivity and porosity is suggested:

$$D_e = \frac{D\phi}{\tau} \quad ,$$

where $D_e$ = effective diffusivity , $D$ = molecular diffusivity , $\phi$ = porosity , and $\tau$ = tortuosity.

## 5.2 One Lump Model Analysis

Two sets of experimental data using sphere S-2 and stirrer speed 1 are plotted in Fig. 5.5 with $[1 - (1/C_s^* + 1)\tilde{T}_f^*]$ vs $\theta$ . The one lump model, Eq. (4.21), suggests a linear relationship between them. As can be seen, the data do not follow a straight line, indicating that the one lump model is not adequate because the internal resistance of rock is neglected.

To take into account the internal resistance, a two lump model or a parametric model may be considered. The two lump model introduces two additional parameters, namely two effective radii. Hunsbedt et al. (1975) have shown that an effective radius depends on the Biot number. In addition, these parameters have no exact physical meaning. Therefore, a parametric model is considered in the following section.

## 5.3 Thermal Diffusivity

The heat transfer experimental data have been matched with Fig. 4.5, developed in Chapter 4, to estimate the value of thermal diffusivity. Experimental data were plotted as $T_f^*$ vs $\theta$ . Figure 4.5 relates $T_f^*$ vs Fr . The Fourier number is related to $\theta$ by the following

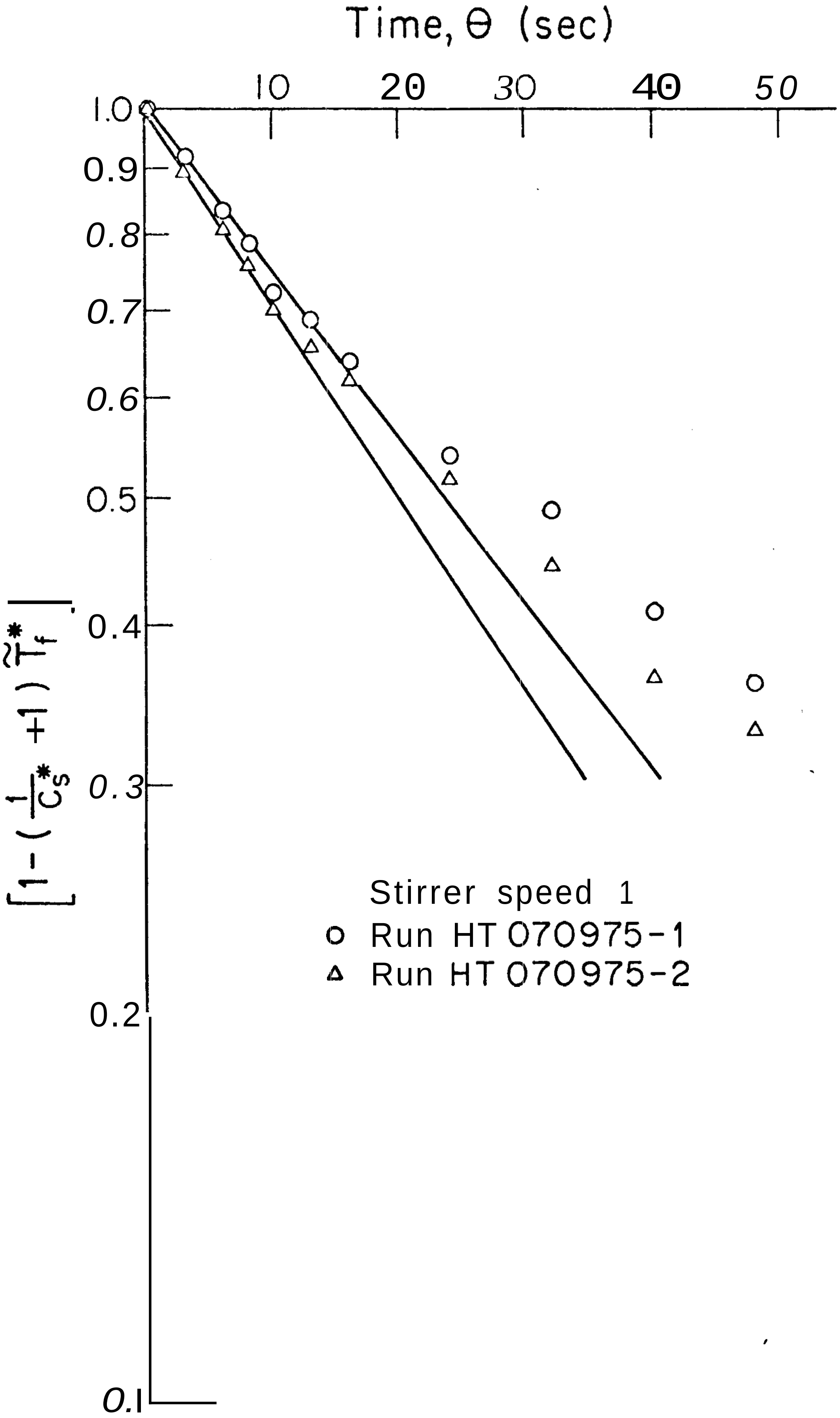

Figure 5.5 Comparison of one lump model with heat transfer experiment data

definition:

$$Fr = \frac{}{R^2} \cdot$$

Taking the logs for both sides, we obtain

$$\log Fr = \log \theta + \log \frac{\alpha}{R^2} .$$

For a given sphere, $\alpha$ and $R$ are constants, and, therefore, log Fr always differs from Log $\theta$ by a coinstant. The experimental data plotted on log-log paper can be shifted from left to right parallelly at the top of Fig. 4.5 to get the best match. From the match point, thermal diffusivity is calculated.

Figures 5.6, 5.7, and 5.8 show the results of the matching. As can be seen, the present model witlhout skin effect cannot fit the experimental data for the whole period of time. Incorporating skin effect into the present model would improve the matching. Table 5.1 summarizes the thermal diffusivity evaluated from several runs. It indicates that the measurement is reproducible; the experimental setup is reliable and will be useful for thermal diffusivity measurement, when the mathematical model is further improved.

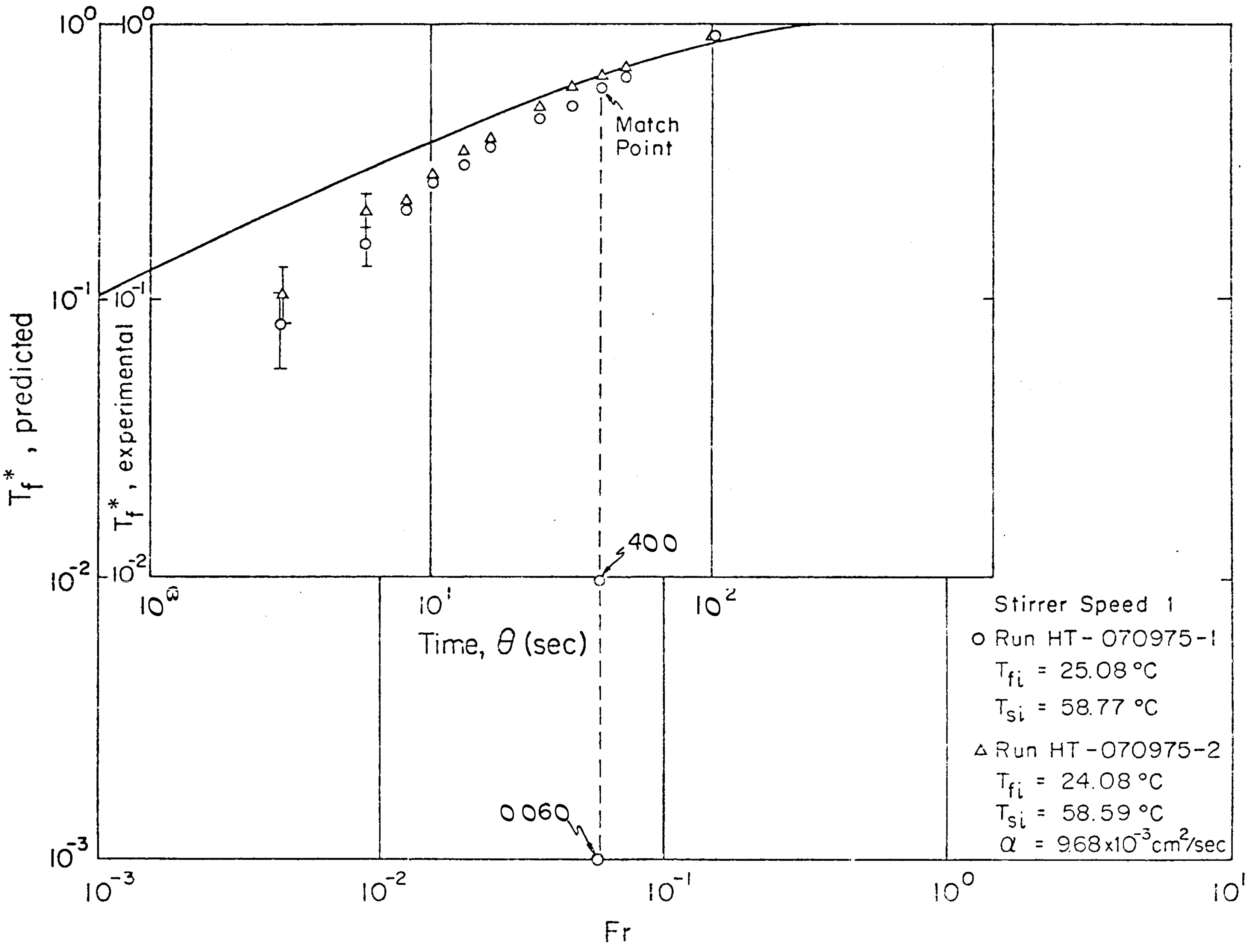

Figure 5.6 Type curve matching for Runs HT-070975-1 and HT-070975-2

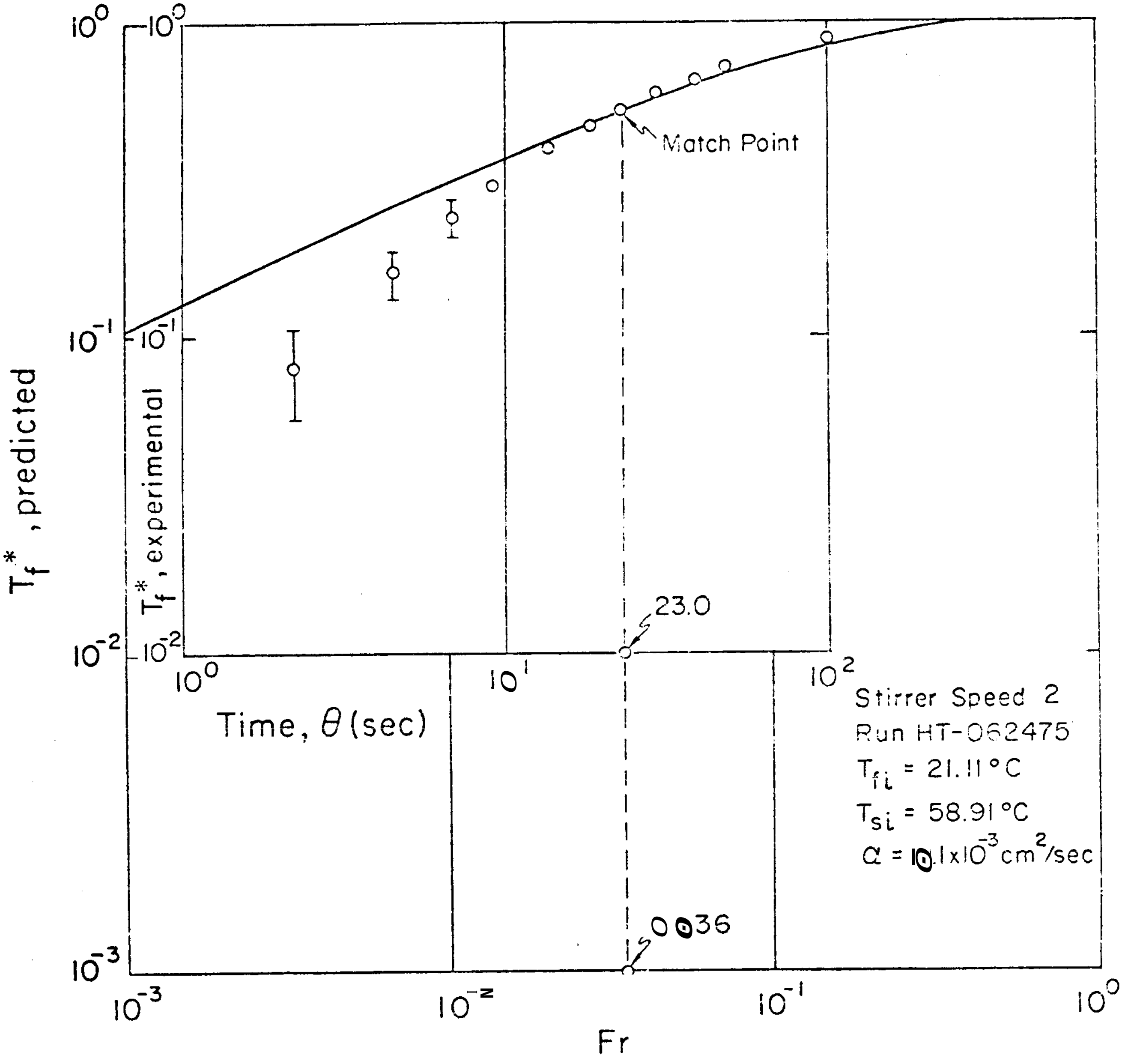

**Figure 5.7** Type curve matching for Run HT-062475

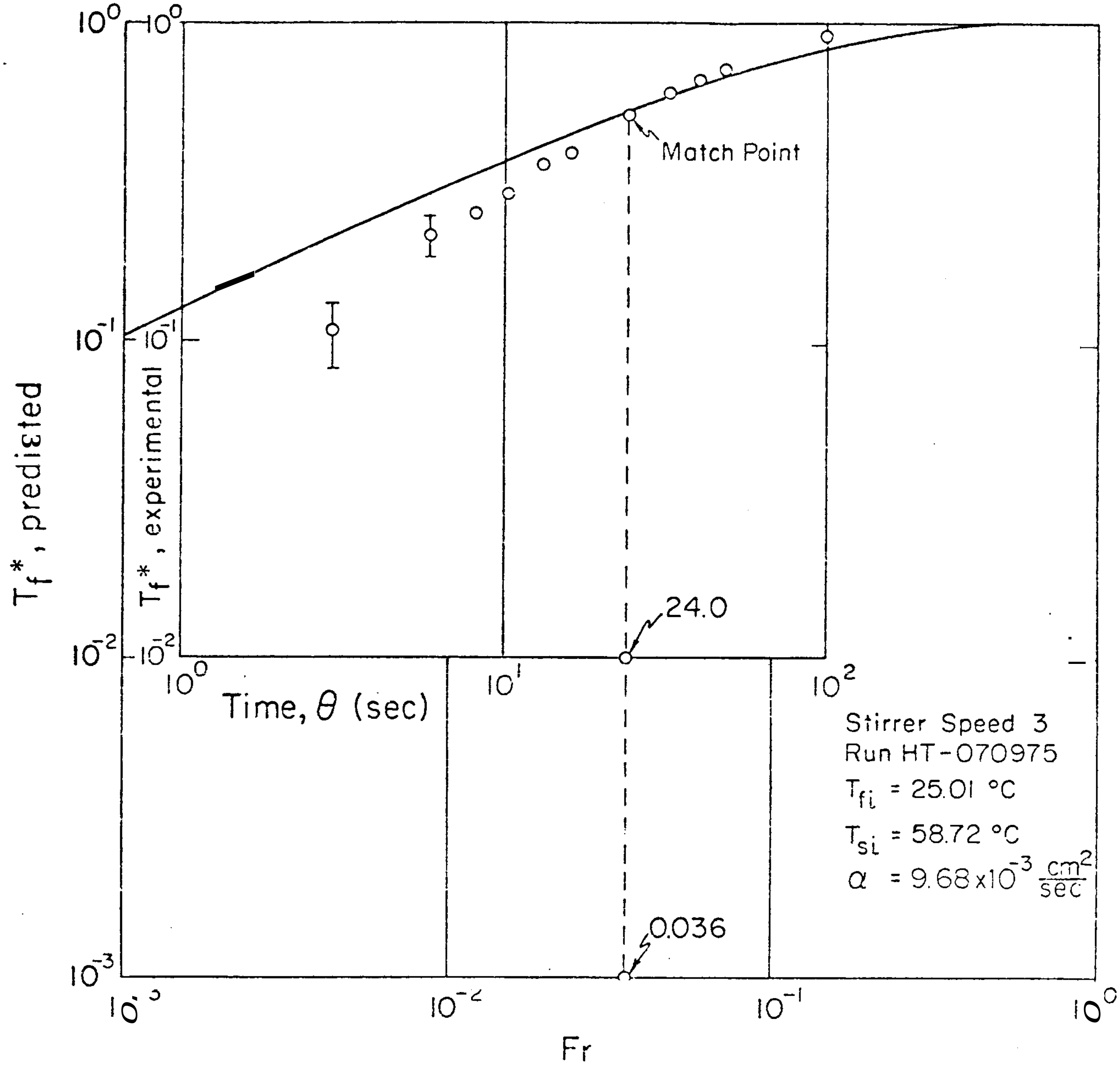

Figure 5.8 Type curve matching for Run HT-070975

## TABLE 5.1

Summary of Data from Heat Transient Experiments

| Run ID No. | Stirrer Speed | Determined $\alpha$ ($\times 10^{-3}$ cm$^2$/sec) |
|---|---|---|
| HT-070975-1<br>HT-070975-2 | 1 | 9.68 |
| HT-062475 | 2 | 10.1 |
| HT-070975 | 3 | 9.68 |
| | | Mean = $9.82 \times 10^{-3}$ cm$^2$/sec. |

# CHAPTER 6

## ASSESSMENT OF EFFECT OF MASS TRANSFER ON ENERGY TRANSFER

Experiments have been carried out for both mass transfer and heat transfer from a single porous rock to the surrounding fluid. Energy transfer due to both heat and mass transfer mechanisms are analyzed. The transport process is divided into two steps: (1) intrasphere transport, and (2) interface: transport. It is considered that heat transfer is the dominant mechanism for energy transfer from a hot porous sphere to the surrounding fluid.

### 6.1 Intrasphere Transport

Heat transfer inside the porous sphere is primarily carried out by the conduction of micropore water and the rock matrix. The so-called "effective conduction" is used for this mechanism. This intrasphere effective conduction process can be well described by the following mathematical model:

$$\frac{\partial T_s}{\partial \theta} = \alpha \frac{1}{r^2} \frac{\partial}{\partial r} \left( r^2 \frac{\partial T_s}{\partial r} \right) , \qquad (6.1)$$

where $T_s$ = the temperature of the sphere , $\alpha$ = the effective thermal diffusivity of the porous sphere, saturated with water , $\theta$ = time , and r = the distance from the center of the porous sphere.

Mass transfer inside the porous sphere is mainly due to molecular self-diffusion of the micropore water. The rate of this process can be characterized by a parameter, $D_e$ , which is the effective diffusivity. The intrasphere mass transfer process can be represented by a mathematical model similar to Eq. (6.1):

$$\frac{\partial C_s}{\partial \theta} = D_e \frac{1}{r^2} \frac{\partial}{\partial r} \left( r^2 \frac{\partial C_s}{\partial r} \right) , \qquad (6.2)$$

where $C_s$ = the concentration of tritiated water, and $D_e$ = the intrasphere effective diffusivity of tritiated water.

It is assumed that no transport resistance exists at the interface when intrasphere transport is considered. Equations *(6.1)* and *(6.2)* can be respectively written in dimensionless variables;, as in the following equations:

$$\frac{\partial T_s}{\partial \theta_h^*} = \frac{1}{r^{*2}} \frac{\partial}{\partial r^*} \left( r^{*2} \frac{\partial T_s^*}{\partial r^*} \right) , \qquad (6.3)$$

$$\frac{\partial C_s^*}{\partial \theta_m^*} = \frac{1}{r^{*2}} \frac{\partial}{\partial r^*} \left( r^{*2} \frac{\partial C_s^*}{\partial r^*} \right) , \qquad (6.4)$$

where

$$T_s^* = \frac{T_s - T_{fi}}{T_{si} - T_{fi}} ,$$

$$C_s^* = \frac{C_s - C_{fi}}{C_{si} - C_{fi}} ,$$

$$\theta_h^* = \frac{\alpha\theta}{r^2} ,$$

$$\theta_m^* = \frac{D_e \theta}{R^2} ,$$

$$r^* = \frac{r}{R} ,$$

and

R = radius of the porous sphere .

Equations *(6.3)* and *(6.4)* have the same solution. In other words, there should be the same dimensionless times, $\theta_h^*$ and $\theta_m^*$ , required for reaching the following conditions, respectively,

$$(T_s - T_{fi}) = 0.1(T_{si} - T_{fi}) ,$$

and

$$(C_s - C_{fi}) = 0.1(C_{si} - C_{fi}) ,$$

i.e., $\theta_h = \theta_m$ .

The effective thermal diffusivity, $\alpha$ , has been estimated at $9.82 \times 10^{-3} \mathrm{cm}^2/\mathrm{sec}$ . The effective diffusivity of tritiated water, $D_e$ , has been estimated around $4.0 \times 10^{-6} \mathrm{cm}^2/\mathrm{sec}$ from experimental data. Therefore, the ratio of real times required for reaching $(T_s - T_{fi}) = 0.1(T_{si} - T_{fi})$ and $(C_s - C_{fi}) = 0.1(C_{si} - C_{fi})$ is:

$$\frac{\theta_h}{\theta_m} = \frac{D_e}{\alpha} = \frac{4.0 \times 10^{-6}}{9.82 \times 10^{-3}} = 4.07 \times 10^{-4} .$$

This suggests that the heat transfer mechanism is accomplished much faster than the mass transfer mechanism.

## 6.2 Interface Transport

Forced heat convection from a sphere can be predicted by the following empirical relation (Bird, 1960):

$$\frac{h_t D}{k_f} = 2.0 + 0.6 \left(\frac{D v_\infty \rho_f}{\mu_f}\right)^{1/2} \left(\frac{C_p \mu}{k}\right)_f^{1/3} , \qquad (6.5)$$

where

$$\frac{h_t D}{k_f} = \overline{Nu} ,$$

$$\frac{Dv_\infty \rho_f}{\mu_f} = Re \ ,$$

and

$$\frac{C_\rho \mu}{k} = Pr \ .$$

Equation (6.5) predicts **Nu** = 2 for a motionless fluid. The subscript "f" represents the property of the fluid. Similarly, forced mass transfer from a sphere can be predicted by the following empirical relation (Bird, 1960):

$$\frac{h_m D}{D_e} = 2.0 + 0.6 \left(\frac{Dv_\infty \rho_f}{\mu_f}\right)^{1/2} \left(\frac{\mu}{\rho D_e}\right)^{1/3} \ , \tag{6.6}$$

where

$$\frac{h_m D}{D_e} = Sh \ ,$$

and

$$\frac{\mu}{\rho D_e} = Sc \ .$$

Equation (6.6) also predicts Sh = 2.0 for a motionless fluid.

A limiting case, where the fluid is motionless, is considered to compare the relative importance of mass and heat transfer mechanisms for interface energy transfer at a low Re region. For this case, we can obtain the following relation from Eqs. (6.5) and (6.6):

$$Nu = Sh = 2.0$$

or

$$\frac{h_t D}{k_f} = \frac{h_m d}{D_e} = 2.0 \ .$$

The numerical values used for the physical constants are as follows:

$$D = 2 \text{ in} = 5.08 \text{ cm} \ ,$$

$$k_f = 0.343 \text{ Btu/hr-ft}^\circ\text{F} \ ,$$

$$\rho_f = 62.4 \text{ lb/ft}^2 = 1.0 \text{ g/cm}^3 \ ,$$

$$D_e = 4.0 \times 10^{-6} \text{cm}^2\text{/sec} \ ,$$

$$C_p = 1.0 \text{ Btu/lb}^\circ\text{F} \ ,$$

and

$$\mu = 2.42 \text{ lb/ft-hr} = 10^{-2} \text{g/cm-sec} \ .$$

Therefore, both heat and mass transfer coefficients can be calculated as follows:

$$h_t = \frac{2.0k_f}{D} = \frac{2.0 \times 0.343 \text{ Btu/hr-ft}^\circ\text{F}}{2 \times 1/12 \text{ ft}} = 4.12 \text{ Btu/hr-ft}^{20}\text{F} \ , \qquad (6.7)$$

$$h_m = \frac{2.0D_e}{D} = \frac{(2.0)(4.0 \times 10^{-6} \text{ cm}^2\text{/sec})}{5.08 \text{ cm}} = 1.57 \times 10^{-6} \text{cm/sec}$$

$$= 1.85 \times 10^{-4} \text{ft/hr} \ . \qquad (6.8)$$

The energy transport due to the heat transfer mechanism, $q_t$ , can be written as

$$q_t = h_t A \Delta T \ . \qquad (6.9)$$

The energy transport due to the mass transfer mechanism, $q_m$ , has been derived in Appendix C and can be written as

$$q_m = h_m A \Delta T \rho_f C_p \ . \qquad (6.10)$$

The ratio of energy transfer due to these two different mechanisms can be obtained from Eqs. (6.9) and (6.10):

$$\frac{q_t}{q_m} = \frac{h_t}{h_m \rho_f C_p} \quad . \qquad (6.11)$$

From Eqs. (6.7), (6.8), and (6.9), $q_t/q_m$ can be calculated:

$$\frac{q_t}{q_m} = \frac{h_t}{h_m \rho_f C_p} = \frac{4.12}{(1.85 \times 10^{-4})(62.4)(1.0)} = 357 \quad .$$

The above ratio suggests that energy transfer at the interface in a low Re region is mainly contributed by the heat transfer mechanism. The mass transfer mechanism, by comparison, is negligible.

In the second case, where the flow regime is in a high Re region, the second terms on the right-hand side of Eqs. (6.5) and (6.6) are much larger than 2.0 . Therefore, the following approximations can be obtained:

$$Nu \doteq 0.6(Re)^{1/2}(Pr)^{1/3} \quad ,$$

$$Sh \doteq 0.6(Re)^{1/2}(Sc)^{1/3} \quad ,$$

or

$$\frac{Nu}{Sh} \simeq \frac{(Pr)^{1/3}}{(Sc)^{1/3}} \quad . \qquad (6.12)$$

The numerical values for Pr and Sc of water can be calculated as follows:

$$Pr = \left(\frac{C_p \mu}{k}\right)_f = \frac{(1.0\ Btu/lb\,^\circ F \times 2.42\ lb/ft\text{-}hr)}{0.343\ Btu/hr\text{-}ft\,^\circ F} = 7.06 \quad , \qquad (6.13)$$

$$Sc = \left(\frac{\mu}{\rho D_e}\right)_f = \frac{10^{-2}\ g/cm\text{-}sec}{(1.0\ g/cm^3)(4.0 \times 10^{-6} cm^2/sec)} = 2.5 \times 103 \quad . \qquad (6.14)$$

Substituting Eqs. (6.13) and (6.14) into Eq. (6.12), we obtain:

$$\frac{Nu}{Sh} = \left(\frac{7.06}{2.5 \times 10^3}\right)^{1/3} = 0.141$$

or

$$\frac{(h_t D)/k_f}{(h_m D)/D_e} = 0.141 \ . \qquad (6.15)$$

Rearranging Eq. (6.15) yields

$$\frac{h_t}{h_m} = \frac{0.141 \ k_f}{D_e} \qquad (6.16)$$

The ratio of energy transfer due to these two mechanisms can be calculated from Eqs. (6.11) and (6.16):

$$\frac{q_t}{q_m} = \frac{h_t}{h_m \rho_f C_p} = \frac{0.141 \ k_f}{\rho_f D_e C_p}$$

$$= \frac{0.141(0.343)\text{Btu/hr-ft}^\circ\text{F}}{(1.0\text{g/cm}^3)(4.0 \times 10^{-6}\text{cm}^2/\text{sec})(1.0\text{Btu/lb}^\circ\text{F})(3600\text{sec/hr})(1\text{b}/450\text{g})(30.5\text{cm/ft})}$$

$$= 49.6 \ . \qquad (6.17)$$

Equation (6.17) also suggests that energy transfer at the interface is mainly a result of heat transport, rather than mass transport.

# CHAPTER 7

# CONCLUSIONS AND RECOMMENDATIONS

## 7.1 Conclusions

1. The effective diffusivity of micropore water has been measured in the order of $10^{-6}$ cm$^2$/sec. The effective diffusivity increases with increasing porosity of the rock fragment.
2. The mass transfer mechanism between micropore water and macropore water under conditions of constant pressure is mainly a molecular diffusion process.
3. The thermal diffusivity of the rock fragment saturated with water has been measured in the order of $10^{-2}$ cm$^2$/sec.
4. Heat transfer is the dominant mechanism for energy transfer from a hot porous sphere to the recycling cold fluid.
5. The present heat transfer experimental setup is reliable for the measurement of thermal diffusivity.

## 7.2 Recommendations

1. The present mathematical model assumes that the surface temperature (concentration) is the same as that in the bulk fluid, Incorporating skin effect into the present model is recommended. The model with skin effect has three advantages. First, it will give a better match with experimental data. Second, it conveys information about interface transport. Third, it will be useful in rock characterization studies. There may exist certain correlations among skin coefficient, Fourier number and rock shapes.

2. The present study consideres spherical shapes for rock fragments. Rock fragments derived from explosive stimulation are of irregular shapes. Rate of heat extraction from hot dry rock by circulating cold fluid, influences the temperature of the produced fluid. It is important to know the heat transient behavior of the hot dry rock, especially when the rock size is large. A rock characterization study is recommended for irregularly shaped rocks.

3. Because of the complex geometry of irregular shapes, it is impossible to solve analytically the transient behavior of rock for irregular shapes. To answer the question, What are the heat transient behaviors of rocks for irregular shapes? we propose the following:

   (a) Characterize rationally the heat transient behavior of rocks for regular geometries, such as finite rectangular and cylindrical shapes, and then extend the characterization to rocks of irregular shapes.

   (b) Test and verify the characterizations experimentally using the existing equipment.

4. The conclusion that heat transfer is the dominant mechanism under constant pressure conditions may not be applicable to heat transfer mechanisms in which heat is extracted by flashing water in situ. For in-situ flashing processes, mass transfer in excess of diffusion may occur as a result of the pressure difference existing between the micropores and macropores.

# APPENDIX A

## DERIVATION FOR PSEUDO STEADY STATE MODEL

In Fig. 4.2(b) we assumed a pseudo steady state system and showed the concentration profile in a partially diffused rock at time $t$ . Under these conditions, the rate of diffusion of the tritiated water is given by

$$\frac{dN}{dt} = 4\pi r^2 Q = 4\pi R^2 Q = 4\pi r_c^2 Q_c = \text{constant} , \tag{A.1}$$

where $Q$ = flux of tritiated water through a surface at radius $r$ , $Q$ = flux of tritiated water through the rock surface, and $Q_c$ = flux of tritiated water through the core surface.

The flux of tritiated water through a surface at radius $r$ may be expressed by Fick's law for diffusion, i.e.,

$$Q = D_e \frac{dC_s}{dr} , \tag{A.2}$$

where $D_e$ is the effective diffusion coefficient of water in the rock. The value of $D_e$ should be very sensitive to porosity and permeability of porous media and to the orientation, density and connection of fractures.

Combining Eqs. (A.1) and (A.2), we obtain for $r$ :

$$\frac{dN}{dt} = 4\pi r^2 D_e \frac{dC_s}{dr} = \text{constant} . \tag{A.3}$$

The condition of a partially diffused rock can be obtained by integrating the above equation from $R$ to $r_c$ :

$$\frac{dN}{dt} \int_R^{r_c} \frac{dr}{r^2} = 4\pi D_e \int_{C_f}^{C_c} dC_s \tag{A.4}$$

or

$$\frac{dN}{dt}\left(\frac{1}{R}-\frac{1}{r}\right) = 4\pi D_e(C_c - C_b) \;. \qquad (A.5)$$

Next, the core size changes with time. Since dN/dt is constant only for a given size of core, as the core shrinks, dN/dt will decrease. The decrease of tritiated water in the core, dN , is related to $dr_c$ by

$$dN = \frac{4}{3}\pi C_c\, d(r_c3) = 4\pi C_c r_c^2 dr_c \;. \qquad (A.6)$$

Replacing $dN_A$ in **Eq.** (A.5) by **Eq. (A.6),** we obtain,

$$C_c r_c^2\left(\frac{1}{R}-\frac{1}{r_c}\right)\frac{dr}{dt} = D_e(C_c - C_b) \qquad (A.7)$$

or

$$C_c\left(\frac{1}{R}-\frac{1}{r_c}\right)r_c^2 dr_c = D_e(C_c - C_b)\,dt \;. \qquad (A.8)$$

Integrating from time 0 to time t , we obtain:

$$\int_{r=R}^{r_c}\left(\frac{1}{R}-\frac{1}{r_c}\right)r_c^2 dr_c = D_e\int_0^t (C_c - C_b)dt \;. \qquad (A.9)$$

Thus, from **Eq.** (A.9), we obtain the following expression for effective diffusivity:

$$D_e = \frac{C_c R^2[1 - 3(r_c/R)^2 + 2(r_c/R)3]}{6\int_0^t (C_c - C_b)\,dt} \qquad (A.10)$$

**In Eq.** (A.10) the effective core radius $r_c$ can be related to measurable quantities through **a** material balance for the tritiated water. The tritiated water exists in three phases, namely core, currounding fluid, and the layer between the core and the surrounding fluid.

Since the core concentration, $C_c$, is constant and the external fluid concentration, $C_b$, can be measured, only the distribution of tritiated water in the intermediate layer needs to be determined. The distribution of tritiated water concentration inside the intermediate layer can be obtained through the material balance equation. The pseudo steady state material balance of tritiated water in intermediate layer at time t results in the following equation:

$$\frac{d^2C}{dr^2} + \frac{2}{r}\frac{dC}{dr} = 0 \qquad \text{(A. 11)}$$

subject to boundary conditions,

$$C = C_f \, , \quad \text{at} \quad r = R \, , \qquad \text{(A. 12)}$$

$$C = C_c \, , \quad \text{at} \quad r = r_c \, . \qquad \text{(A. 13)}$$

Solving Eqs. (A.11), (A.12), and (A.13), we obtain:

$$C = \frac{C_c - C_f}{1/r_c - 1/R}\,\frac{1}{r} + \frac{RC_f - r_c C_c}{R - r_c} \qquad \text{(A. 14)}$$

The initial amount of tritiated water in the rock is given by

$$N_i = \frac{4}{3}\pi R^3 C_c \, .$$

At any instant t, the total amount of tritiated water is distributed in the core, surrounding fluid, and porous layer. The amount inside the core is $4/3\pi r_c^3 C_c$. The amount in the surrounding fluid is $N_f = C_f V$, where V is the volume of surrounding fluids. The amount in the porous layer can be obtained from the following integration:

$$N = \int_{r_c}^{R} C 4\pi r^2 dr$$

$$= \int_{r_c}^{R} 4\pi r^2 \left[ \frac{C_c - C_f}{1/r_c - 1/R} \frac{1}{r} + \frac{RC_f - r_c C_c}{R - r_c} \right] dr$$

$$= \frac{2\pi (C_c - C_f)}{1/r_c - 1/R} (R^2 - r_c^2) + \frac{4\pi (RC_f - r_c C_c)}{3(R - r_c)} (R^3 - r_c^3) .$$

Therefore the material balance for tritiated water in the system can be written as

$$\frac{4}{3} \pi R^3 C_c = \frac{4}{3} \pi r_c^3 C_c + C_f V + \frac{2\pi (C_c - C_f)}{1/r_c - 1/R} (R^2 - r_c^2)$$

$$+ \frac{4\pi (RC_f - r_c C_c)}{3(R - r_c)} (R^3 - r_c^3) \qquad \text{(A. 15)}$$

or

$$\frac{4}{3} \pi C_c (R^3 - r_c^3) = C_f V + \frac{2\pi (C_c - C_f)}{(1/r_c - 1/R)} (R^2 - r_c^2)$$

$$+ \frac{4\pi (RC_f - r_c C_c)}{3(R - r_c)} (R^3 - r_c^3) . \qquad \text{(A. 16)}$$

The above equation relates the measurable quantities, $C_c$ , $C_f$ , $R$ and $V$ , to the effective core radius $r_c$ for a pseudo steady state model. The effective diffusivity, $D_e$ , can be calculated from Eqs. **(A.10)** and **(A.16)** from known values of $R$ , $V$ , $C_c$ and measuring $C_f$ as a function of time.

# APPENDIX B

## DERIVATION FOR EQUATIONS (4.8) AND (4.9) OR EQUATIONS (4.27) AND (4.28)

A transformation $Z = r^*X$ is introduced into Eqs. (4.6) and (4.7), or (4.25) and (4.26). A set of two linear partial differential equations with constant coefficients are obtained:

$$\frac{\delta Z}{\delta \theta^*} = \frac{\delta^2 Z}{\delta r^{*2}} ,$$

$$\frac{dY}{d\theta^*} = 3\omega\left(\frac{\delta Z}{\delta r^*} - Z\right)\bigg|_{r^*=1}$$

The initial and boundary conditions become:

1. When $\theta^* = 0$ ,

$$Z = 0 ,$$

$$C_f^* = 1 .$$

2. At $r^* = 1$ ,

$$Z = Y , \text{ for } \theta^* > 0 .$$

3. At $r^* = 0$ ,

$$Z = 0 , \text{ for } \theta^* > 0 .$$

The Laplace transformation of the above system equations and the initial and boundary conditions with respect to $\theta^*$ yields:

$$s\bar{Z} = \frac{d^2\bar{Z}}{dr^{*2}} , \tag{B.1}$$

$$s\bar{y} - 1 = -3\omega\left(\frac{d\bar{Z}}{dr^*} - \bar{Z}\right)\bigg|_{r^*=1} , \tag{B.2}$$

subject to:

1. $\bar{Z}(s,1) = \bar{Y}(s)$ ;
2. $\bar{Z}(s,0) = 0$ .

Solving Eq. (B.1), $\bar{Z}$ can be written as

$$\bar{Z} = a_1 e^{s^{1/2} r*} + a_2 e^{s^{1/2} r*} , \qquad (B.3)$$

where $a_1$ and $a_2$ are arbitrary constants and can be determined through the boundary conditions. From Eq. (B.3) and boundary condition (2), it can be obtained that:

$$a_1 + a_2 = 0 .$$

Therefore, $\bar{Z}$ can be given as:

$$\bar{Z} = a_1 (e^{s^{1/2} r*} - e^{s^{1/2} r*}) = 2a_1 \sinh(s^{1/2} r*) . \qquad (B.4)$$

Applying Eqs. (B.2) and (B.4) and boundary condition (1), $a_1$ can be determined to be

$$a_1 = \frac{1}{2[(s - 3\omega) \sinh(s^{1/2}) + 3\omega s^{1/2} \cosh(s^{1/2})]} .$$

Substituting $a_1$ into Eq. (B.4), $\bar{Z}$ becomes

$$Z = \frac{\sinh(s^{1/2} r*)}{[(s - 3\omega) \sinh(s^{1/2}) + 3\omega s^{1/2} \cosh(s^{1/2})]} .$$

$\bar{X}$ can be obtained through the transformation introduced, $\bar{X} = 1/r*(\bar{Z})$ ,

$$\overline{X}(s,r^*) = \frac{\sinh(s^{1/2}r^*)}{r^*[(s-3\omega)\sinh(s^{1/2}) + 3\omega s^{1/2}\cosh(s^{1/2})]}$$

$$= \frac{\sinh(s^{1/2}r^*)/\sinh(s^{1/2})}{r^*[(s-3\omega) + 3\omega s^{1/2}\coth(s^{1/2})]} \ . \qquad \text{(B.5)}$$

The inverse Laplace transforms of $\overline{X}$ can be obtained by means of the residue theory (Wylie, 1960):

$$\mathcal{L}^{-1}\{\overline{X}(s,r^*)\} = \sum \text{ residue of } \overline{X}(s,r^*)\, e^{s\theta^*} \qquad \text{(B.6)}$$

at each of its poles. $\overline{X}(s,r^*)$ has a first-order pole at $s = 0$. Moreover, $\overline{X}(s,r^*)$ has infinitely many other first-order poles, namely, the points where

$$\frac{s}{3\omega} - 1 + s^{1/2}\coth(s^{1/2}) = 0 \ .$$

$s$ must be negative in order to be physically feasible, or, the points where $s = -\gamma_n^{\,2}$, and $\gamma_n$ satisfies $y \cot \gamma = 1 + \gamma^2/3\omega$, and,

$n = 1,2,\ldots,\infty$,

at $s = 0$ the residue of $\overline{X}(s,r^*)\, e^{s\theta^*}$ is :

$$\lim_{s \to 0} \frac{s^* \sinh(s^{1/2}r^*)\, e^{s\theta^*}}{r^*[(s-3\omega)\sinh(s^{1/2}) + 3\omega s^{1/2}\cosh(s^{1/2})]} = \frac{1}{\omega + 1} \ ;$$

at $s = -\gamma_n^{\,2}$, the residue of $\overline{X}(s,r^*)\, e^{s\theta^*}$ is :

$$\lim_{s \to -\gamma_n^2} \frac{(s + \omega_n 2)\sinh(s^{1/2}r^*)\, e^{s\theta^*}}{r^*[(s-3\omega)\sinh(s^{1/2}) + 3\omega s^{1/2}\cosh(s^{1/2})]}$$

$$= \frac{2\sin(\gamma_n r^*)\, e^{-\gamma_n^2\theta^*}}{r^*\sin(\gamma_n)\,[(3\omega + 3) + (\gamma_n^{\,2})/3\omega]} \ .$$

Hence, the inverse Laplace transform of $\bar{X}(s,r^*)$ can be obtained by summing the above residues:

$$X(\theta^*,r^*) = \mathcal{L}^{-1}\{\bar{X}(s,r^*)\} = \sum \text{residues of } \bar{X}(s,r^*)\ e'^* \quad \begin{array}{l}\text{at each of}\\ \text{its poles}\end{array}$$

$$= \frac{1}{\omega + 1} + \frac{2}{r^*} \sum_{n=1}^{\infty} \frac{\sin(\gamma_n r^*)\ e^{-\gamma_n^2 \theta^*}}{\sin(\gamma_n)[(3\omega + 3) + \gamma_n^2/3\omega]} \tag{B.7}$$

$Y(\theta^*)$ equals $X(\theta^*,r^*)$ , when $r^* = 1$ , and can be written as

$$Y(\theta^*) = \frac{1}{\omega + 1} + 2 \sum_{n=1}^{\infty} \frac{e^{-\gamma_n^2 \theta^*}}{[(3\omega + 3) + \gamma_n^2/3\omega]} \ . \tag{B.8}$$

## APPENDIX C

## DERIVATIONS FOR EQUATION (6.10)

The mass transfer rate equation for self-diffusion of tritiated water from the sphere to the surrounding fluid can be represented by

$$\dot{m}_{tr} = h_m(C_s - C_{bulk})\,A\rho_f \,,$$

where $\dot{m}_{tr}$ = the self-diffusion rate of the tritiated water from the sphere to the surrounding fluid , $h_m$ = the mass transfer coefficient , $C_s$ = the concentration of the tritiated water at the interface , $C_i$ = the initial concentration of the tritiated water inside the sphere , A = the surface area of the sphere , and $\rho_f$ = the density of the tritiated water or water . At the beginning;, $C_{bulk} = 0$ , and $C_s = C_i$ . Therefore ,

$$\dot{m}_{tr} = h_m C_i A\rho_f \;.$$

Defining $\dot{m}_L$ as the self-diffusion rate of the water from the sphere to the surrounding fluid, and $\dot{m}_R$ as the self-diffusion rate of the water from the surrounding fluid to the sphere, because it is an exchange process, $\dot{m}_L = \dot{m}_R$ . The self-diffusion rate of the water is $1/C_i$ times greater than the self-diffusion rate of the tritiated water, because only a portion of the micropore water is labeled, and can be represented by

$$\dot{m}_L = \dot{m}_R = \frac{1}{C_i}\,\dot{m}_{tr} = h_m A\rho_f \;.$$

The energy transfer rate due to $\dot{m}_L$ can be expressed as

$$\dot{q}_L = \dot{m}_L C_p T_s = h_m A \rho_f C_p T_s \quad ,$$

while the energy transfer rate due to $\dot{m}_R$ can be written as

$$\dot{q}_R = \dot{m}_R C_p T_f = h_m A \rho_f C_p T_f \quad .$$

Therefore, the net energy transfer rate due to self diffusion can be expressed as

$$\dot{q} = \dot{q}_L - \dot{q}_R = h_m A \rho_f C_p \Delta T \quad .$$

# APPENDIX D

## DATA OF MASS TRANSFER EXPERIMENT

Mass Transfer Experiment, Run No. MT-121074

Temperature = °C

Stirrer Speed 2

'water in cylinder = 3250 mℓ

$C_{bg}$ = 11 cpm/mℓ

'dry ball = 126.3 g

$C_{fi}$ = 21 cpm/mℓ

$W_{sat'd\ ball}$ = 141 g

$C_{bi} = 2.0 \times 10^5$ cpm/mℓ

$W_{HTO\ soaked}$ = 14.7 g

$$C_{f\infty} = \frac{W_{HTO\ soaked} \times C_{bi}}{\text{''water in cylinder}} = 905 \text{ cpm/m}\ell$$

$R_{ball}$ = 1.0 in = 2.54 cm

$$C_f^* = \frac{C_f - C_{fi}}{C_{f\infty} - C_{fi}}$$

$\phi$ = 0.214

| θ,min | | $C_f$,cpm/mℓ | | $C_f^*$ |
|---|---|---|---|---|
| 0 | | 21.0 | | |
| 12 | | 57.1 | | 0.0408 |
| 20 | | 68.6 | | 0.0539 |
| 30 | | 81.6 | | 0.0686 |
| 40 | | 101.1 | | 0.0906 |
| 53 | | 111.4 | | 0.1020 |
| 64 | | 131.2 | | 0.1250 |
| 90 | | 158.3 | | 0.1550 |
| 121 | | 182.4 | | 0.1830 |
| 152 | | 212.9 | | 0.2170 |
| 180 | | 234.6 | | 0.2420 |
| 272 | | 247.2 | | 0.2560 |
| 360 | | 334.6 | | 0.3550 |
| 415 | | 344.6 | | 0.3660 |
| 475 | | 349.8 | | 0.3720 |
| 517 | | 378.2 | | 0.4040 |
| 722 | | 440.3 | | 0.4740 |
| 1450 | | 561.2 | | 0.6110 |
| 3305 | | 68'7.7 | | 0.7540 |
| 4707 | | 801.3 | | 0.8830 |
| 5930 | | 797.0 | | 0.8780 |
| 7418 | | 886.0 | | 0.9790 |
| 8792 | | 881.0 | | 0.9730 |
| 10175 | | 90.3.0 | | 0.9980 |
| 11625 | | 926.0 | | 1.0200 |
| 14500 | | 926.0 | | 1.0200 |
| .8800 | | 924.0 | | 1.0200 |

## Mass Transfer Experiment, Run No. MT-071775

Temperature = °C

Stirrer Speed 2

'water in cylinder = 2250 mℓ

$C_{bg}$ = 11.3 cpm/mℓ

$W_{dry\ ball}$ = 154.8 g

$C_{fi}$ = 64 cpm/mℓ

'sat 'd ball = 143.4 g

$C_{bi}$ = 1.5 x $10^5$ cpm/mℓ

$W_{HTO\ soaked}$ = 11.4 g

$$= \frac{W_{HTO\ soaked} \times C_{bi}}{\text{'water in cylinder}}$$

$R_{ball}$ = 1.0 in = 2.54

$\bar{C}_f$ = mean of $C_f$

$\phi$ = 0.166

$$C_f^* = \frac{\bar{C}_f - C_{fi}}{C_{f\infty} - C_{fi}}$$

| θ,min | Vial No. | $C_f$,cpm/mℓ | $\bar{C}_f$,cpm/mℓ | $C_{f\infty}$,cpm/mℓ | $C_f^*$ |
|---|---|---|---|---|---|
| 0 | | | | 760 | |
| 13 | 7 | 102.0 | 95 ± 6 | | 0.0445 ± 0.010 |
| | 8 | 91.6 | | | |
| | 9 | 91.9 | | | |
| 22 | 11 | 108.3 | 107 ± 1 | 763 | 0.0618 |
| | 12 | 106.9 | | | |
| | 13 | 107.1 | | | |
| 32 | 14 | 125.6 | 123 ± 2 | | 0.0848 |
| | 15 | 121.1 | | | |
| | 16 | 123.4 | | | |
| 42 | 21 | 138.9 | 138 ± 1 | 767 | 0.0965 |
| | 22 | 138.7 | | | |
| | 23 | 137.6 | | | |
| 52 | 24 | 149.2 | 157 ± 12 | | 0.121 ± 0.016 |
| | 25 | 150.1 | | | |
| | 26 | 170.6 | | | |
| 63 | 27 | 184.6 | 173 ± 10 | | 0.142 f0.013 |
| | 28 | 168.1 | | | |
| | 29 | 165.6 | | | |
| 240 | 31 | 269.0 | 279 ± 13 | 770 | 0.279 f0.017 |
| | 32 | 275.1 | | | |
| | 33 | 293.4 | | | |
| 335 | 34 | 347.5 | 344 ± 4 | | 0.369 |
| | 35 | 344.0 | | | |
| | 36 | 339.5 | | | |
| 1145 | 37 | 405.5 | 396 ± 17 | | 0.431 f0.022 |
| | 38 | 375.8 | | | |
| | 39 | 405.3 | | | |

cont.

cont.

| θ,min | Vial No. | $C_f$, cpm/mℓ | $\bar{C}_f$, cpm/mℓ | $C_{f\infty}$, cpm/mℓ | $C_f^*$ |
|---|---|---|---|---|---|
| 1650 | 42 | 548.8 | 570 ± 30 | 774 | 0.654 f0.039 |
| | 43 | 591.2 | | | |
| 4588 | 44 | 776.7 | 765 ± 18 | | 0.906 ± 0.023 |
| | 45 | 774.1 | | | |
| | 46 | 744.1 | | | |
| 6875 | 47 | 946.4 | 894 ± 45 | | 1.07 ± 0.058 |
| | 48 | 866.5 | | | |
| | 49 | 869.4 | | | |
| 9950 | 54 | 742.0 | 740 ± 47 | 777 | 0.870 ± 0.060 |
| | 55 | 692.0 | | | |
| | 56 | 785.0 | | | |
| 11450 | 57 | 887.8 | 859 ± 100 | | 1.02 f0.129 |
| | 58 | 747.9 | | | |
| | 59 | 942.1 | | | |
| 13025 | 61 | 858.9 | 794.7 ±60 | 781 | 0.934 f0.077 |
| | 62 | 784.2 | | | |
| | 63 | 741.0 | | | |
| 15765 | 64 | 816.9 | 788 ± 26 | | 0.927 ± 0.033 |
| | 65 | 765.8 | | | |
| | 66 | 781.1 | | | |
| 17015 | 67 | 762.2 | 744 ± 19 | | 0.871 ± 0.024 |
| | 68 | 724.4 | | | |
| | 69 | 744.0 | | | |

Mass Transfer Experiment, **Run** No. MT-073175

Temperature = °C

$W_{\text{water in cylinder}}$ = 2250 mℓ

$W_{\text{dry ball}}$ = 229.3 g

$W_{\text{sat'd ball}}$ = 266.4 g

$W_{\text{HTO soaked}}$ = 37.1 g

$R_{\text{ball}}$ = 1.25 in = 3.18 cm

$\phi = 0.277$

Stirrer Speed 2

$C_{bg}$ = 11.6 cpm/mℓ

$C_{fi}$ = 30 cpm/mℓ

$C_{bi}$ = 1.50 X $10^5$ cpm/mℓ

$$C_{f\infty} = \frac{W_{\text{HTO soaked}} \times C_{bi}}{W_{\text{water in cylinder}}}$$

$\bar{C}_f$ = mean of $C_f$

$$C_f^* = \frac{\bar{C}_f - C_{fi}}{C_{f\infty} - C_{fi}}$$

cont.

cent.

| θ,min | | $C_f$,cpm/mℓ | $\bar{C}_f$,c m/mℓ | $C_{f\infty}$,cpm/m | $C_f^*$ |
|---|---|---|---|---|---|
| 0 | | | | 2473 | |
| i5 | | 172.2 | 174 ± 2 | | 0.0589 |
| | | 175.8 | | | |
| 27 | | 244.0 | 251 ± 11 | | 0.0905 ± 0.005 |
| | | 245.8 | | | |
| | | 264.3 | | | |
| 48 | | 296.3 | 297 ± 1 | | |
| | | 298.0 | | | |
| | | 295.2 | | | |
| 180 | | 557.6 | 567 ± 8 | 2496 | 0.218 |
| | | 570.6 | | | |
| | | 572.6 | | | |
| 260 | | 676.3 | 679 ± 12 | | 0.263 |
| | | 669.1 | | | |
| | | 692.8 | | | |
| 470 | | 970.0 | 919 ± 46 | | 0.361 ± 0.019 |
| | | 880.7 | | | |
| | | 905.1 | | | |
| 1250 | | 1531.9 | 1523 ± 107 | 2507 | 0.603 ± 0.043 |
| | | 1624.6 | | | |
| | | 1411.6 | | | |
| 2750 | | 1854.2 | 1881 ± 65 | | 0.747 ± 0.026 |
| | | 1955.2 | | | |
| | | 1832.9 | | | |
| 4115 | | 2099.7 | 2073 ± 23 | | 0.825 |
| | | 2057.0 | | | |
| | | 2063.0 | | | |
| 5620 | | 2239.3 | 2240 ± 81 | 2518 | 0.888 ± 0.033 |
| | | 2321.1 | | | |
| | | 2159.5 | | | |
| 6965 | | 2281.3 | 2315 ± 51 | | 0.918 50.021 |
| | | 2290.2 | | | |
| | | 2373.8 | | | |
| 8410 | | 2364.2 | 2255 ± 153 | | 0.894 f0.062 |
| | | 2320.8 | | | |
| | | 2080.6 | | | |
| 9910 | | 2689.3 | 2626 ± 64 | 2530 | 1.038 ± 0.026 |
| | | 2560.7 | | | |
| | | 2628.1 | | | |
| 11315 | | 2506.7 | 2421 ± 83 | | 0.956 ± 0.033 |
| | | 2415.7 | | | |
| | | 2341.9 | | | |
| 12715 | | 2737.6 | 2636 ± 111 | | 1.042 ± 0.044 |
| | | 2517.5 | | | |
| | | 2652.4 | | | |
| 14340 | | 2634.3 | 2595 ± 49 | 2541 | 1.022 ± 0.020 |
| | | 2610.5 | | | |
| | | 2539.5 | | | |
| 15615 | | 2435.3 | 2419 ± 68 | | 0.951 ± 0.027 |
| | | 2344.2 | | | |
| | | 2477.4 | | | |

# APPENDIX E

## DATA OF HEAT TRANSFER EXPERIMENT

Heat Transfer Experiment, Run No. HT-070975-1

$T_{fi} = 23.08\,^{\circ}C$

Stirrer Speed 1

$$\frac{1}{\omega} = \frac{T_{si} - T_{fi}}{T_{f\infty} - T_{fi}} = 57.56$$

$T_{si} = 58.77\,^{\circ}C$

$$(T_f - T_{fi})\ \mathrm{cor.} = (T_f - T_{fi}) + \frac{dT}{d\theta}$$

$$\frac{dT}{d\theta} = \frac{0.01}{100}\ ^{\circ}C/\mathrm{sec}$$

$$T_f^* = \frac{(T_f - T_{fi})\ \mathrm{cor.}}{T_{f\infty} - T_{fi}}$$

$$\tilde{T}_f^* = \frac{T_f - T_{fi}}{T_{si} - T_{fi}}$$

| $\theta$,sec | $T_f - T_{fi}$, °C | $(T_f - T_{fi})$ cor., °C | $T_f^*$ | $1-(1/\omega + 1)\,\tilde{T}_f^*$ |
|---|---|---|---|---|
| - 200 | - 0.04 | | | |
| - 100 | - 0.03 | | | |
| 0 | 0 | 0 | 0.0000 | 1.000 |
| 2.9 | 0.05 | 0.05 | 0.0806 | 0.918 |
| 5.8 | 0.10 | 0.10 | 0.161 | 0.836 |
| 8 | 0.13 | 0.13 | 0.210 | 0.787 |
| 10.2 | 0.16 | 0.16 | 0.258 | 0.719 |
| 13.1 | 0.19 | 0.19 | 0.307 | 0.689 |
| 16 | 0.22 | 0.22 | 0.355 | 0.639 |
| 24 | 0.28 | 0.28 | 0.452 | 0.541 |
| 32 | 0.31 | 0.31 | 0.500 | 0.491 |
| 40 | 0.36 | 0.36 | 0.581 | 0.409 |
| 48 | 0.39 | 0.39 | 0.629 | 0.361 |
| 100 | 0.57 | 0.56 | 0.903 | 0.0812 |
| 200 | 0.63 | 0.61 | 0.984 | 0.00079 |
| 300 | 0.65 | 0.62 | 1.000 | |
| 400 | 0.66 | 0.62 | 1.000 | |
| 500 | 0.67 | 0.62 | 1.000 | |

Heat Transfer Experiment, Run No. HT-070975-2

$T_{fi} = 24.08^\circ C$

**Stirrer Speed 1**

$$\frac{1}{\omega} = \frac{T_{si} - T_{fi}}{T_{f\infty} - T_{fi}} = 58.49$$

$T_{si} = 58.59^\circ C$

$$(T_f - T_{fi})\ \text{cor.} = (T_f - T_{fi}) + \frac{dT}{d\theta} \cdot \theta$$

$$\frac{dT}{d\theta} = \frac{0.01}{100}\ ^\circ C/\text{sec}$$

$$T_f^* = \frac{(T_f - T_{fi})\ \text{cor.}}{T_{f\infty} - T_{fi}}$$

$$\tilde{T}_f^* = \frac{T_f - T_{fi}}{T_{si} - T_{fi}}$$

| $\theta$,sec | $T_f - T_{fi}$, °C | $(T_f - T_{fi})$ cor. ,°C | $T_f^*$ | $1-(1/\omega + 1)\ \tilde{T}_f^*$ |
|---|---|---|---|---|
| - 200 | - 0.04 | | | |
| - 100 | - 0.03 | | | |
| 0 | 0 | 0 | 0.000 | 1.0 |
| 2.9 | 0.06 | 0.06 | 0.102 | 0.897 |
| 5.8 | 0.11 | 0.11 | 0.186 | 0.810 |
| 8 | 0.14 | 0.14 | 0.237 | 0.759 |
| 10.2 | 0.17 | 0.17 | 0.288 | 0.707 |
| 13.1 | 0.20 | 0.20 | 0.339 | 0.655 |
| 16 | 0.22 | 0.22 | 0.373 | 0.621 |
| 24 | 0.28 | 0.28 | 0.475 | 0.517 |
| 32 | 0.32 | 0.32 | 0.542 | 0.448 |
| 40 | 0.37 | 0.37 | 0.627 | 0.363 |
| 48 | 0.39 | 0.39 | 0.661 | 0.328 |
| 100 | 0.57 | 0.56 | 0.949 | 0.0345 |
| 200 | 0.60 | 0.58 | 0.983 | 0.00057 |
| 300 | 0.62 | 0.59 | 1.000 | |
| 400 | 0.63 | 0.59 | 1.000 | |
| 500 | 0.64 | 0.59 | 1.000 | |

## Heat Transfer Experiment, Run No. HT-062475

$T_{fi} = 21.11\,^{\circ}C$

Stirrer Speed 2

$$\frac{1}{\omega} = \frac{T_{si} - T_{fi}}{T_{f\infty} - T_{fi}} = 60.00$$

$T_{si} = 58.91\,^{\circ}C$

$$(T_f - T_{fi})\ \text{cor.} = (T_f - T_{fi}) + \frac{dT}{d\theta}\cdot\theta$$

$$\frac{dT}{d\theta} = \frac{0.01}{100}\ ^{\circ}C/sec$$

$$T_f^* = \frac{(T_f - T_{fi})\ \text{cor.}}{T_{f\infty} - T_{fi}}$$

$$\tilde{T}_f^* = \frac{T_f - T_{fi}}{T_{si} - T_{fi}}$$

| θ,sec | $T_f - T_{fi}$, °C | $(T_f - T_{fi})$ cor., °C | $T_f^*$ | $1-(1/\omega + 1)\tilde{T}_f^*$ |
|---|---|---|---|---|
| - 200 | - 0.05 | | | |
| - 100 | - 0.04 | | | |
| 0 | 0 | 0 | 0.00 | 1.00 |
| 2.2 | 0.05 | 0.05 | 0.0794 | 0.919 |
| 4.5 | 0.10 | 0.10 | 0.159 | 0.838 |
| 6.8 | 0.15 | 0.15 | 0.238 | 0.758 |
| 9.1 | 0.19 | 0.19 | 0.302 | 0.693 |
| 13.6 | 0.25 | 0.25 | 0.397 | 0.597 |
| 18.2 | 0.29 | 0.29 | 0.460 | 0.532 |
| 22.7 | 0.33 | 0.33 | 0.524 | 0.467 |
| 29.5 | 0.37 | 0.37 | 0.587 | 0.404 |
| 38.6 | 0.41 | 0.41 | 0.651 | 0.338 |
| 47.7 | 0.45 | 0.45 | 0.714 | 0.274 |
| 100 | 0.56 | 0.55 | 0.873 | 0.112 |
| 200 | 0.64 | 0.62 | 0.984 | 0.0004 |
| 300 | 0.66 | 0.63 | 1.000 | |
| 400 | 0.67 | 0.63 | 1.000 | |
| 500 | 0.68 | 0.63 | 1.000 | |

Heat Transfer Experiment, **Run** No. HT-070975-3

$T_{fi} = 25.01\,^{\circ}\text{C}$ Stirrer Speed **3**

$$\frac{1}{\omega} = \frac{T_{si} - T_{fi}}{T_{f\infty} - T_{fi}} = 59.14 \qquad T_{si} = 58.72\,^{\circ}\text{C}$$

$$(T_f - T_{fi})\text{ cor.} = (T_f - T_{fi}) + \frac{dT}{d\theta}\cdot\theta \qquad \frac{dT}{de} = \frac{0.01}{LOO}\,^{\circ}\text{C/sec}$$

$$T_f^* = \frac{(T_f - T_{fi})\text{ cor.}}{T_{f\infty} - T_{fi}} \qquad \tilde{T}_f^* = \frac{T_f - T_{fi}}{T_{si} - T_{fi}}$$

| $\theta$,sec | $T_f - T_{fi}$, °C | $(T_f - T_{fi})$ cor., °C | $T_f^*$ | $1-(1/\omega + 1)\tilde{T}_f^*$ |
|---|---|---|---|---|
| - 200 | | | | |
| - 100 | | | | |
| 0 | 0 | 0 | 0.000 | 1.00 |
| 2.9 | 0.06 | 0.06 | 0.1015 | 0.893 |
| 5.8 | 0.12 | 0.12 | 0.211 | 0.786 |
| 8 | 0.14 | 0.14 | 0.246 | 0.75 |
| 10.2 | 0.16 | 0.16 | 0.281 | 0.715 |
| **13.1** | 0.20 | 0.20 | 0.351 | 0.643 |
| 16 | 0.22 | 0.22 | 0.386 | 0.607 |
| 24 | 0.29 | 0.29 | 0.509 | 0.483 |
| 32 | 0.34 | ***0.34*** | 0.594 | 0.393 |
| 40 | 0.37 | 0.37 | 0.64'9 | 0.340 |
| 48 | 0.40 | 0.40 | 0.702 | 0.286 |
| 100 | 0.53 | 0.53 | 0.912 | 0.0726 |
| 200 | 0.58 | 0.56 | 0.983 | 0.00167 |
| 300 | 0.60 | 0.57 | 1.000 | |
| *400* | 0.61 | 0.57 | 1.000 | |
| 500 | 0.62 | 0.57 | 1.0010 | |

# REFERENCES

1. Arihara, N., "A Study of Non-Isothermal Single and Two-Phase Flow through Consolidated Sandstones," Stanford Geothermal Program Technical Report No. 2, Nov. 1974.

2. Austin, C. F. and Leonard, G. W., "Chemical Explosive Stimulation of Geothermal Wells," in Geothermal Energy, Kruger and Otte (eds.), Stanford University Press, 1973.

3. Bird, R. B., Stewart, W. E. and Lightfoot, E. N., Transport Phenomena, John Wiley and Sons, Inc., 1960.

4. Burnham, J. B. and Stewart, D. H., "Recovery of Geothermal Energy from Hot, Dry Rock with Nuclear Explosives," in Geothermal Energy, Kruger and Otte (eds.), Stanford University Press, 1973.

5. Carslaw, H. S. and Jeager, J. C., Conduction of Heat in Solids, Oxford at the Clarendon Press, 1959.

6. Crank, J., The Mathematics of Diffusion, Oxford University Press, London, 1956.

7. Ewing, A. H., "Stimulation of Geothermal Systems," in Geothermal Energy, Kruger and Otte (eds.), Stanford University Press, 1973.

8. Heath, L. J., "Variations in Permeability and Porosity of Synthetic Oil Reservoir Rock--Method of Control," Soc. Pet. Enpr. J., 329, Dec. 1965.

9. Horrocks, D. L., "Measuring of Tritium with Liquid Scintillation Systems," in Tritium, Moghissi and Carter (eds.), Messenger and Graphics Publishers, 1973.

10. Hunsbedt, A., Kruger, P. and London, A. L., "A Laboratory Model of Stimulated Geothermal Reservoirs," Stanford Geothermal Program Technical Report No. 7, Feb. 1975.

11. Kelly, H. L. and Phillips, C. R., "Review of Tritium Monitoring Devices," in Tritium, Moghissi and Carter (eds.), Messenger and Graphics Publishers, 1973.

12. Kruger, P., Principles of Activation Analysis, Wiley Interscience, 1971.

13. Kruger, P. and Ramey, H. J., Jr., "Stimulation and Reservoir Engineering of Geothermal Resources," Stanford Geothermal Program Technical Report No. 1, June 1974.

14. Ramey, H. J., Jr., Kruger, P. and Raghavan, R., "Explosive Stimulation of Hydrothermal Reservoirs," in Geothermal Energy, Kruger and Otte (eds.), Stanford University Press, 1973.

15. Smith, M., Potter, R., Brown, D. and Aamodt, R. L., "Induction and Growth of Fractures in Hot Rock," in Geothermal Energy, Kruger and Otte (eds.), Stanford University Press, 1973.

16. United States Department of Interior, Final Environmental Impact Statement for the Geothermal Leasing Program, Vol. I, 1974.

17. Wang, J. H., Robinson, C. V. and Edelman, I. S., "Self-Diffusion and Structure of Liquid Water. III. Measurement of the Self-Diffusion of Liquid-Water with $H^2$, $H^3$ and $O^{18}$ as Tracers," J. Amer. Chem. Soc., Vol. 75, 466, 1953.

18. Wygal, R. J., "Construction of Models that Simulate Oil Reservoirs," Soc. Pet. Engr. J., 281, Dec. 1963.